MASARYK UNIVERSITY
Faculty of Science
Department of Physical Electronics

Ph.D. Dissertation

Brno 2023 Michael Kroker

MASARYK UNIVERSITY
Faculty of Science
Department of Physical Electronics

Magnetron sputtered hard ternary coatings with enhanced fracture toughness

Ph.D. Dissertation

Michael Kroker

Supervisor: prof. Mgr. Petr Vašina, Ph.D. **Brno 2023**

Bibliographic Entry

Author:	Mgr. Michael Kroker Faculty of Science, Masaryk University Department of Physical Electronics
Title of Thesis:	Magnetron sputtered hard ternary coatings with enhanced fracture toughness
Degree Programme:	Physics
Field of Study:	Plasma Physics
Supervisor:	prof. Mgr. Petr Vašina, Ph.D.
Academic Year:	2022/2023
Number of Pages:	xi + 130
Keywords:	W-B-C, Ta-B-C, protective coatings, magnetron sputtering, deposition process

Bibliografický záznam

Autor:	Mgr. Michael Kroker Přírodovědecká fakulta, Masarykova univerzita Ústav fyzikální elektroniky
Název práce:	Magnetronové naprašování tvrdých ternárních vrstev se zvýšenou lomovou houževnatostí
Studijní program:	Fyzika
Studijní obor:	Fyzika plazmatu
Vedoucí práce:	prof. Mgr. Petr Vašina, Ph.D.
Akademický rok:	2022/2023
Počet stran:	xi + 130
Klíčová slova:	W-B-C, Ta-B-C, ochranné vrstvy, magnetronové naprašování, depoziční proces

Abstract

The state-of-the-art hard protective coatings suffer from low fracture and damage resistance because they are based on brittle ceramic materials. It limits the coating resilience and, therefore, the lifespan of the coated tools. Recently, a new type of material was proposed by quantum mechanical calculations to overcome this drawback. The ternary systems of metal, boron, and carbon atoms allegedly provide a combination of stiffness and moderate ductility. The thesis is a comprehensive experimental study of these novel materials prepared as coating under industrial conditions by magnetron sputtering. It is based on joint research of the Masaryk University and the Czech coating manufacturer SHM, s.r.o., which specializes in commercial coating of tools. The research yields the properties of tantalum- and tungsten-based coatings prepared in industrial batch-coater. It describes the influence of elemental and phase composition on the coating's mechanical properties and also shows the aspects of the industrial deposition process. The thesis introduces the research, provides fundamentals for the reader to understand the ground of the work, and compiles the author's publications. Prints of the publications are included and commented on.

Abstrakt

Aktuálně využívané tvrdé ochranné vrstvy založené na keramických materiálech trpí nízkou odolností proti lomu a poškození, což při mechanickém namáhání limituje životnost povlakovaných nástrojů. V nedávné době byla na základě kvantově mechanických výpočtů navrhnuta nová kategorie materiálů, které tuto nevýhodu nevykazují. Takové ternární povlaky, obsahující kov, bor a uhlík, by měly vykazovat tuhost a zároveň zvýšenou lomovou houževnatost. V disertační práci jsou povlaky připraveny v průmyslovém měřítku metodou magnetronového naprašování a následně studovány. Výzkum vznikl ve spolupráci Masarykovy univerzity a české společnosti SHM, s.r.o., která komerčně povlakuje nástroje. Práce se zaměřuje na studium vlastností vrstev obsahujících tantal a wolfram, vliv fázového a prvkového složení vrstev na jejich mechanické vlastnosti a zároveň na aspekty jejich průmyslové přípravy. Práce také poskytuje principiální základy, uvádí do výzkumu a shrnuje předcházející poznatky. Disertační práce je kompilátem autorových publikací sepsaných v rámci doktorského studia a jejich komentářů.

Poděkování

Na tomto místě bych rád vyjádřil poděkování prof. Mgr. Petru Vašinovi, Ph.D., který mě provedl nástrahami doktorského studia a směroval tento výzkum ke kýženým výsledkům svými rozsáhlými zkušenostmi a odbornými radami. Díky jeho vedení vznikla práce, která nepostrádá smysl a posunula vědění dále. Také bych rád vyzdvihl tým průmyslového partnera SHM, s.r.o., který poskytl nejen experimentální zařízení pro výzkum, ale především spolehlivou technickou podporu. Děkuji všem, kteří se na tomto výzkumu podíleli, ať už sdílením svých širokých znalostí, technických zkušeností, nebo experimentální prací. Jmenovitě bych rád zmínil doc. Mgr. Pavla Součka, Ph.D., doc. RNDr. Vilmu Buršíkovou, Ph.D. a Mgr. Lukáše Zábranského, Ph.D., jakožto konzultanty této disertace. Vážím si také podpory rodiny a mé partnerky, kteří byli vždy oporou mých studií a výzkumné práce.

Prohlášení

Prohlašuji, že jsem disertační práci vypracoval samostatně pod vedením prof. Mgr. Petra Vašiny Ph.D. s využitím poznatků doktorského výzkumu, odborných publikacích, ke kterým jsem přispěl a informačních zdrojů, které jsou v práci citovány.

Brno 21. listopad 2022 . . . .

Michael Kroker

Contents

Preface

This text serves as the dissertation for Plasma Physics doctoral studies at Masaryk University. The thesis aims to introduce to the reader the topic and present the findings derived from the doctoral research. It compiles the author's original publications and commentaries, connecting the research conclusions to a broader perspective with a background provided by the accompanying text.

The thesis follows the author's doctoral research of ternary metal-boron-carbon coatings and the study of the industrial deposition process based on magnetron sputtering. The research is a joint effort of Masaryk University and coating manufacturer SHM, s.r.o., which specializes in tool coating. Their portfolio includes several types of protective coatings applicable for machining, forming, die casting, and more.

The first chapter of the thesis provides an insight into the fundamentals of sputtering and points out the differences between laboratory and industrial research. Chapter 2 presents the rationale behind the metal-boron-carbon coatings with a description of their properties and introduces two non-trivial methodologies particularly adapted for their characterization. Chapter 3 describes how the deposition process modeling can connect and ease the research efforts and further provide a tool for deploying the technology in the industry. The final chapter contains prints of the author's publications on which the thesis is based and a list of co-authored publications, including bibliographic entries and statements of the author's contribution. The publications are referred to as follows:

- **4.1** On the origin of multilayered structure of W-B-C coatings prepared by non-reactive magnetron sputtering from a single segmented target
- **4.2** Composition, structure and mechanical properties of industrially sputtered Ta-B-C coatings
- **4.3** Industrially deposited hard and damage resistant W-B-C coatings
- **4.4** Predicting the composition of W-B-C coatings sputtered from industrial cylindrical segmented target
- **4.5** Co-authored publications

Introduction

A thin film or coating is a layer of material applied to an object to alter its surface properties. That, although correct, but vaguely stated definition includes many cases and techniques, which fundamentals are to put a layer of material onto any object, like painting, spraying, electroplating, etc. The advances in vacuum technologies and the invention of the sputtering process developed a solid ground to prepare thin films differently. Building the thin films atom by atom widened the range of materials that can be prepared on the surface and opened new possibilities for applications. The term *thin* is of high importance here. The thin film with thickness ranging from several nanometers to a few micrometers is sufficient to substantially alter the surface properties, i.e., electrical, optical, protective, or mechanical properties. From the integrated circuits over engines to mirrors, thin films have become part of everyday technological life and are essential for many industrial branches.

Material sciences are the backbone of thin film development as they provide the theoretical description and the means of investigation and direct the research toward novel materials. However, in the end, the success of technologies is dictated by real-world applications, and coating technologies are no exception. The benefits of applying the coating must outweigh the work and cost investments and advance the field further. The focus on novel materials and new coating technologies is thus driven mainly by industrial demand.

Joint research between academia and industry boosts the research and development process significantly. The academia provides extensive knowledge and a rigorous approach, while the industry aids technological issues and, with its broad experience, points the research toward faster deployment of the technology. Noted that neither the academia nor the industry lacks the said abilities, but in joint research, both parties benefit.

The ternary metal-boron-carbon (Me-B-C) coatings possess the potential to exhibit high hardness while maintaining moderate ductility and thus limiting the probability of failure due to brittle fracture. Despite the potential applicability, the research of industrially deposited Me-B-C coatings is sporadic. The goal of the doctoral research is thus to assess the feasibility of industrial manufacturing and map the properties of the Me-B-C coatings deposited on the industrial batch coater. Therefore, ease the future deployment of these coatings in manufacturing production.

Chapter 1

Industrial magnetron sputtering

1.1 Fundamentals

Thin film deposition from the vapor phase took a giant leap in the early 1800s with the advances in vacuum technologies. The vapor deposition usually takes place in an environment of low pressure, which enables effortless transport of small particles and limits the contamination from the ambient atmosphere. The vapor phase is composed of small particles that condensate on the substrate creating a thin film. The vapor phase may be obtained in several ways, but two basic classes can be distinguished.

If the method is based on chemical processes like the dissociation of precursors, reduction/oxidation reactions, and others, it sorts as chemical vapor deposition (CVD). Alternatively, the process is physical and classifies as physical vapor deposition or PVD. The physical methods include evaporation, ablation, and sputtering. However, the basic principle of each one is to overcome the surface binding energy of the material to release and deposit its parts onto the substrate. During the evaporation, the material is heated to sublimation temperature, which spontaneously releases the particles into volume. Another form is arc evaporation, which is based on arc discharge. The high current of the arc concentrated into the cathode spot overheats the material, vaporizes it, and rapidly ejects it toward the substrate as the vapor expands. The ablation, on the other hand, relies on a short, intense laser pulse that overheats the material.

Sputtering is a phenomenon that takes place when an accelerated atom collides with the matter. The atom transports through the matter while transferring the momentum and energy into the inner structure until stopped or recoiled. This leads to the collision cascade – a set of consecutive momentum and energy transfers within the atomic structure of matter. With a certain probability, the collision cascade results in the ejection of the particle from the surface. The ejected particles are individual atoms, molecules, or their clusters.

Experimentally the sputtering can be performed in the evacuated chamber using a beam of ions pointed toward solid matter – a target. The ions are accelerated to sufficient energies by electric field. The efficiency of sputtering can be defined as the ratio between the number of ejected atoms to the number of incident ions, the so-called sputtering yield. The sputtering yield depends on the atomic masses of target atoms and incidence ions, the binding energy between the target atoms, material density, the energy of the incidence ions, and the angle under which they impinge on the target.

The sputtering also occurs in the glow discharges as a consequence of plasma interacting with the cathode. The fall of the voltage in the cathode region causes positive gas ions to accelerate toward the cathode and hit it. If the energy threshold for sputtering is met, the atoms of the cathode material are ejected, which can be observed as the gradual erosion of the cathode and by the thin film formed on the inner side of the discharge tube. This setup is the base for a technique called diode sputtering. The substrate is placed on the anode, the cathode acts as the target, and the plasma ionizes the discharge gas, which is the source of the positive ions and is thus called the working gas.

Endless strive for higher deposition efficiency and quality of films advanced the sputtering further. The magnetron sputtering was invented by adding the magnets to the setup creating the magnetic field above the target. The electron trajectory is prolonged due to Lorentz force, and the electrons perform orbital motion around the magnetic field lines, trapping them near the target. The plasma density is increased above the target, which favors more intense sputtering. Consequently, the pressure of the working gas can be reduced, thus increasing the mean free path of sputtered particles. The magnetic field is not homogeneously distributed, which causes the target to be not eroded evenly, and the erosion trench (racetrack) develops. Figure 1.1a shows typical configuration of the magnetic field above target. The region of increased plasma density is where the magnetic field lines are parallel to the target. The region is visible during the deposition process by more intensive glow on the sputter source as shown in figure 1.1b. It corresponds to the erosion of target (figure 1.1c).

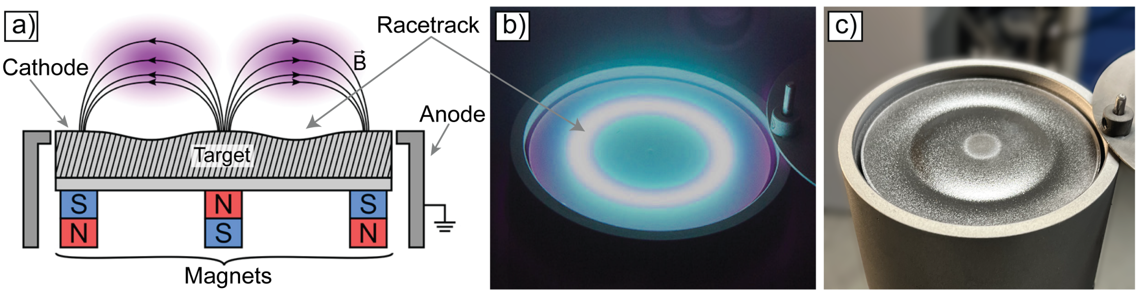

Figure 1.1: a) Schematic of planar magnetron sputter source according to [1] and images of b) active sputter source and c) target with visible erosion trench mounted on sputter source.

Although the momentum transfer is most effective if the mass of the incident ion equals the mass of the target atom, the choice of working gas also affects other parameters. To not change the target chemically during sputtering, the working gas and its fragments should not unintentionally react with it. Moreover, efficient ionization of the gas is preferred, and the energy should not be dissipated to vibrational and rotational energy states.

The mono-atomic structure of the rare inert gasses possesses the said properties, and they are, unambiguously, a common choice for magnetron sputtering. Argon is most often utilized as the all-purpose working gas, because it has considerably high atomic mass to sputter most materials effectively and is cost-effective as well. However, in certain cases, it is also utilized helium, neon or krypton.

In addition to the inert working gas, the molecular reactive gas can be added during the sputtering process. The gas molecules dissociate, excite, and undergo other reactions

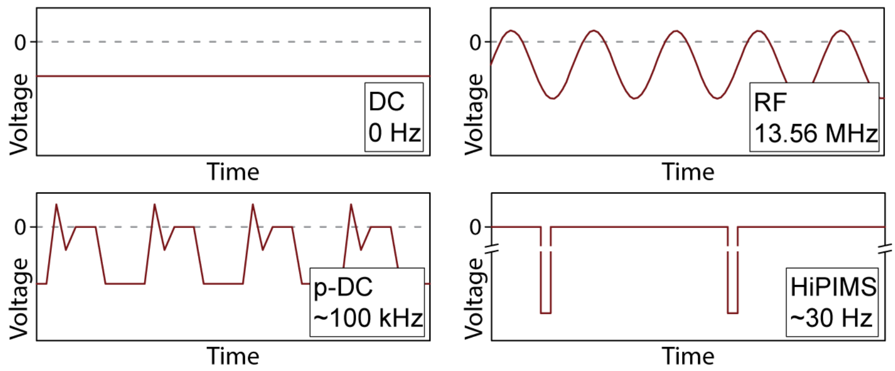

Figure 1.2: Time-dependent evolution of voltage for several types of power supplies.

described by the plasma chemistry and thus can react with target atoms to create compounds. The so-called reactive sputtering enables synthesizing and depositing materials like nitrides, carbides, oxides, and more, expanding the set of materials that can be prepared by magnetron sputtering. Adding the reactive gas, however, makes the sputtering process far more challenging to control, and feedback control is often required.

The sputtering is initiated by applying a high voltage to the target in the evacuated chamber. If the breakdown condition is met, the plasma is ignited above the target and sustained by the electric power supply through capacitive coupling. The target is the cathode, and the surrounding chamber and substrates are the grounded anode. Noting the substrate may be biased to different potential to control the energy of incoming ions. Several kinds of power supplies have been developed so far and can be distinguished by the time evolution of the supplied voltage; see figure 1.2.

During the direct current magnetron sputtering (dcMS), the power is delivered continuously to plasma, and the charge is carried through the target by electrons and ions. If the charge cannot transfer through, it is accumulated on the surface, resulting in strong electric fields and unwanted arcing. Arcing can also occur due to target contamination or debris in the racetrack. The large current spike concentrated in a very small area may damage the power supply and locally overheat the target. Arc protection is thus often employed, which quickly reacts to the arc occurrence and suppresses the arcing by a short break of power input [2].

The non-conductive materials can be sputtered by alternating the voltage polarity. The positive parts of the cycle release the accumulated charge and prevent arcing. Typically are utilized radio-frequency power supplies that operate with a frequency 13.56 MHz. Radio-frequency magnetron sputtering (rfMS) is flexible and can be utilized for sputtering all materials. However, it requires extra components to adjust the impedance of the transmission line in order not to reflect the power back to the supply [2].

Other pulsed power supplies are also known. For example, mid-frequency pulsed direct current (p-DC) supplies operate typically on frequencies 50-350 kHz. These supplies often feature a positive overshoot of voltage at the end of each pulse, which can increase the amount and mean energy of ions bombarding the substrate during the deposition process [3]. Recent developments also led to the invention of HiPIMS (high power impulse magnetron sputtering), which is based on short, very intense pulses with a small duty cycle. The HiPIMS increases the ionization fraction of sputtered atoms and the energy of deposited particles, which improve the coating properties and may result in denser coatings when compared to dcMS [4, 5].

The magnetron sputtering is flexible technique, that enables to synthesise many materials and prepare them in form of thin film. Basically no constraints apply for the target, or the substrate. The low temperature plasma enables to prepare materials without thermodynamic equilibrium with substrate, thus heat sensitive substrates can also be sputter deposited onto. The deposited power (or energy influx) can, however, still be controlled independently. The energy of arriving ions can be controlled by the bias voltage applied to substrate, and the substrate can often be heated. This is crucial because, processes such as diffusion, growth mode, phase formation, crystallization etc. depend on the energy available at the substrate surface [6, 7].

1.2 Thin films applications

Thin films are commonly employed as a cost-efficient way to alter the surface properties and preserve the bulk properties of the substrate. Since the 1980s, most commercial thin films have been prepared either by arc evaporation or magnetron sputtering [8]. The thin film design is always based on the intended use.

The electrical properties of thin films can be tuned. Depending on the thin film material, one can obtain highly conductive metallic films utilized in fine electronics or non-conductive oxide films used as insulators [9]. Available are also transparent conductive thin films based on oxides utilized in the flexible displays or solar cells [10, 11]. The applications take advantage of the thin films' optical properties as well. The anti-reflective lenses, optical filters, mirrors, etc. usually utilize surface treatments, which are often based on complex, multilayered films [12]. The food industry employs barrier coatings for polymer packaging, which limit the transition rates of oxygen, water vapor, and other chemicals and increase thus the shelf life of products [13, 14].

Coatings are broadly used as a protective layer, which purpose is to endure the surrounding environment, preserve the substrate properties and protect it. The coatings may provide a protective barrier in chemically harsh environments. Surface coated with chemically stable material prevents the corrosive substances from reaching the substrate so the corrosion reactions cannot start and the substrate is preserved [15].

Chemically and thermally stable coatings with small thermal conductivity can be utilized, for example, as a thermal barrier and protection of the substrate from high-temperature environments. The chemical stability and thermal barrier are utilized in turbines, where the coatings reduce the heat transfer from the high-temperature gas to the metal surfaces of the turbine casing and blades. Such coatings reduce corrosion and build-up of compounds originating from the combustion reaction. The lifespan may thus be significantly improved, or the turbine may operate at higher temperatures making it more effective [16].

The essential feature of protective coatings is their mechanical properties. The mechanical properties depend on the entire coating-substrate system as they are exerted under stress, load, or friction. For example, a hard coating applied on the machining tool provides a surface capable of cutting various metals, alloys or compounds but still preserves the bulk properties of the steel [17]. The hard protective coatings enable the high-speed machining, forming, and die casting of materials that would otherwise be impossible.

Coatings and thin films are part of day-to-day modern life, often without our knowledge. A great variety of materials is nowadays utilized for different applications, see the examples in the table 1.1. However, preceding the industrial deployment of any coating is always the material research and development of the deposition process.

Application field	Coating materials
Tooling	TiN, CrN, ZrN, TiCN, TiAlN, AlCrN, TiC, TiB_2, BN, $TiAlN/Si_3N_4$, diamond-like carbon (DLC)
Automotive	MoS_2, WS_2, TiC/amorphous-C, metal doped DLCs
Optics	metals, MgF_2, CaF_2, CeF_3, SiO_2, TiO_2, Ta_2O_5, Al_2O_3, Y_2O_3, HfO_2, ZnS, Ge
Decorations	TiN, ZrN, TaN, HfN, CrCN, TiCN, TiAlN
Microelectronics	metals, TiN, TaN, TiW, InSnO, ZnO:Al, $MoSi_2$, $CoSi_2$, GaN, GaAs, SiO_2, Al_2O_3, Si_3N_4
Optoelectronics	Si, $CuInSe_2$, $CuInGaSe_2$, SnO_2, ZnO:Al, In_2O_3:ZnO, CdS
Biomedicine	DLC, Ta- and Ti-based materials

Table 1.1: Examples of coating materials according to application field [9–12, 17–21].

1.3 Shifting from laboratory research to industrial application

The apparatus designed for magnetron sputtering composes of several parts and subsystems. The chamber is capable of reaching the high vacuum by multistage pumping. The base pressure is typically lower than $5 \cdot 10^{-3}$ Pa to limit the partial pressures of contaminants from ambient air in the chamber and provide the clean deposition process. Controllable intake and gas distribution must be provided, so the gases reach the sputter source and substrate and provide a stable deposition environment.

The operating pressure of working gas ranges from tenth to several Pascals during the magnetron sputtering, which corresponds to the mean free path of sputtered particle 10-15 cm for the lowest pressure and several millimeters for the high operating pressure [22]. Assuming the target-substrate distance of a several centimeters, the sputtered particle usually undergoes a few collisions with the working gas atoms before reaching the substrate. However, the collective motion of sputtered particles from the target can heat the gas and lower the gas pressure locally in front of the sputter source, commonly known as the gas rarefaction [23].

Sputter source designed for magnetron sputtering composes of the target, magnetic field, and cooling. The magnetic field is generated either using coils or, more often, by permanent magnets. The electric supply is connected to the target and powers the plasma. The thermal energy dissipated during sputtering heats the target and the magnets placed in its close vicinity. Water cooling ensures that the temperature of the magnets, target and whole assembly stays at safe levels.

Laboratory systems

In laboratories, scientists benefit from flexible devices, which enable them to research many materials and cover a wide range of deposition conditions, ideally utilizing a single apparatus. The research is often conducted as a parametric study based on observing the influence of process parameters on the properties of the thin film. The deposition process parameter, like substrate temperature, gas pressure, bias voltage, power, and others, serve as the independent variable to which are linked properties of the coating. The values of the process parameters and studied range are chosen wisely based on the theoretical background to attain certain conditions and desirably influence the coating properties.

Manual control of the deposition system is crucial since the process is often researched from scratch. However, automatic logging of parameters is often beneficial if the system is computer-controlled because the deposition may be reviewed afterward and show the subtle effects and hidden dependencies visible only in broader perspective. An example of process log is in figure 1.3. The data log shows the records of process parameters and sensor data from dcMS deposition process including the heating, ion cleaning of substrates, coating deposition and cool down.

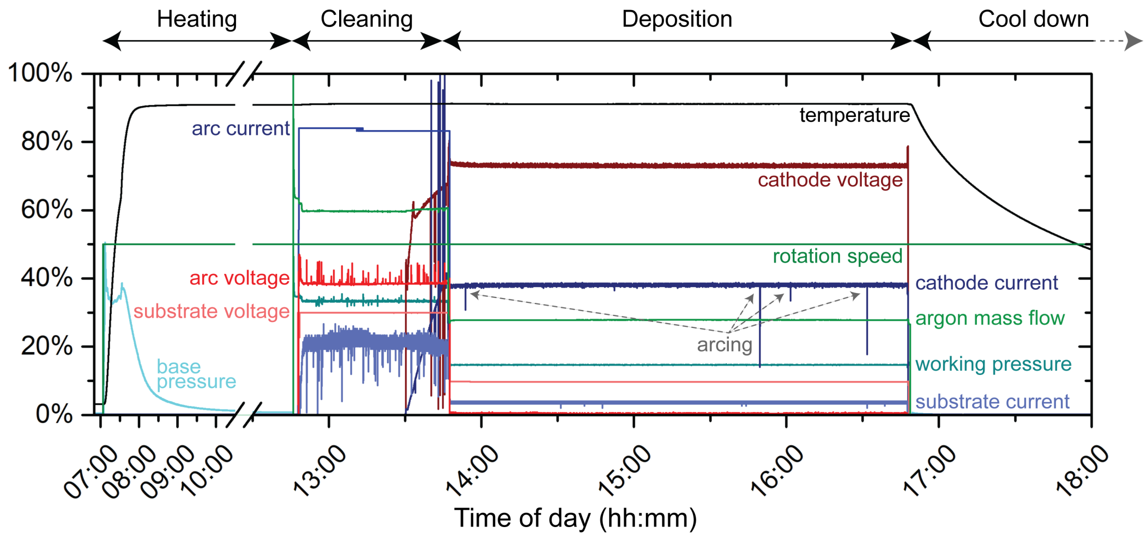

Figure 1.3: Example of parameters and sensors data log. Scale of vertical axis is based on value range and is different for individual parameters.

The typical compact design of the vacuum chamber often provides easy manipulation and short pumping times. With the addition of a load-lock, the low pressure in the chamber is maintained during the substrate loading and unloading, so the deposition chamber is not contaminated.

Commonly the sputter sources are designed to mount flat targets, typically of circular shape with a diameter between 2 to 6 inches. The permanent magnets may be interchangeable to obtain a balanced or unbalanced magnetic field and rearrange the magnetic poles in case of multiple sputter sources. Inverting the pole configuration of neighboring sputter sources results in closed field configuration where the magnetic field lines are connected between the sputter sources [24].

The substrates utilized for laboratory research are of small dimensions and flat. This eases the manipulation and provides access to various analytical methods, which often give restraints on the size of the specimen. The monocrystalline silicon wafer is a common multipurpose substrate, but plastics, steels, or any special substrates like polished carbon, alumina and many more may be used. Substrate material always depends on the intended use and aim of the research.

Industrial systems

Industrial coaters are built with different perspective than laboratory machines. The design is dictated to provide high manufacturing throughput and cost-effective solutions.

The process parameters are usually optimized specifically for each case of deposited material and given substrate. The deposition process must be repeatable and robust to maintain the coating parameters regardless of the daytime, machine, or operator. The batch-coaters are thus usually computer-controlled with software that sets the deposition process parameters and maintains desired order of operation. Various sensors including multiple temperature, pressure and voltage gauges may be used within the coater to monitor the deposition process and ensure its expected behavior.

Industrial coaters can accommodate either a large number of substrates or substrates with considerable dimensions and of various shapes in one batch. The vacuum chamber is of large dimensions and houses substrate holders that often perform multi-axis rotation to ensure uniform coating or are capable of the in-line or roll-to-roll deposition on large format glass sheets and foils.

The sputter sources are designed to operate on a high power level and maximize the utilization of the target. During the deposition, the target's thickness decreases until it can no longer be used and needs to be replaced with a new target. However, due to the plasma density not being distributed evenly, the material utilization is not uniform, see figure 1.4.

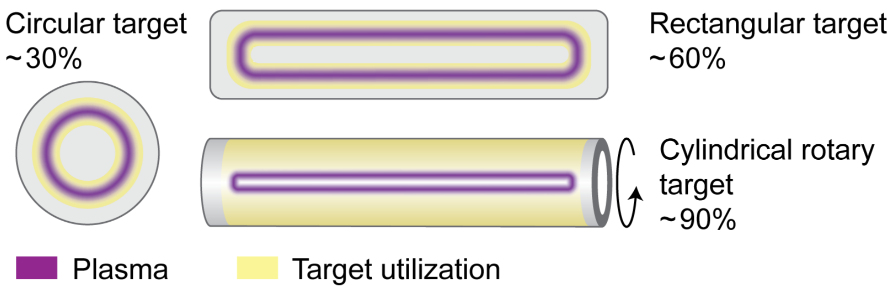

Figure 1.4: Utilization of circular, rectangular and cylindrical rotary targets.

The circular design utilizes about 30% of the target material. Some improvements can be made to increase the utilization by changing the racetrack shape and introducing the special movement of the target. Manufacturers more frequently utilize large rectangular targets with about two times higher utilization than standard circular targets [25]. The highest utilization, however, provide cylindrical rotary targets. The magnetic field is stationary, and the racetrack points towards the substrate, but the target is rotating and thus is sputtered uniformly, attaining the utilization up to 90% [8, 26].

The target material can be either monoatomic or, more often, composed of multiple elements to reduce the number of sputter sources in the system. Once the coating composition is tuned and marked for production manufacturing, the target is manufactured with a specific composition to achieve the wanted properties of the coating. Metals are alloyed and shaped to the required target geometry. Non-alloyable materials can be synthesized by sintering of ceramics or hot-pressing of powder compounds and other methods.

However, such targets sometimes are challenging to utilize for manufacturing coatings as they may develop intrinsic stress and be too brittle to handle effectively. The deposition process must consider the target's thermal and electric conductivity, ability to handle thermal shocks, and other properties [9].

Additionally, good purity of targets must be achieved not to influence the coating properties with other than the intended elements in the structure. The target design belongs to the problematic aspects of coating manufacturing for these reasons.

1.4 Challenges of industrial research

Conducting research on the industrial apparatus and developing the deposition process involves many aspects that must be considered. The industrial sputtering system often does not offer high flexibility because the system controls are usually constrained. Its software is optimized only for a specific sequence of steps and maintains a safe operation.

The industrial sputter sources utilize large format targets, which are usually custom-made. Compound targets are often used, so the single active sputter source is sufficient to deposit desired coatings. But this is not versatile specifically for research of multi-element coatings, where various compositions need to be tested. Attaining a wide range of coating compositions with a single sputter source requires frequent changing of targets. However, supplying a variety of large format targets with different compositions is not cost-effective and takes significant effort to handle.

The research must also follow the constraints on the deposition parameters given by the industrial demand. These apply to the pressure, temperature, power, deposition time, and more. For example, the temperature of certain tool steel cannot be too high because the steel would temper and change properties otherwise. Developing outstanding coating is pointless if the constraints are not fulfilled and the deposition process cannot be deployed for production.

The high power utilized for coating production shortens the deposition times and thus favors the production efficiency, but it can also affect the deposition process. Even though the industrial sputter sources have been optimized to handle the thermal load, the high power density may influence the target's properties and cause irreversible changes, for example, re-crystallization of metal targets, which influences the sputtering yield of the target [27]. Such effects are often hidden in corresponding laboratory research.

The purity of the deposition process has to be also considered. The utilized materials and gases may contain impurities and also the history of the sputtering system may influence the deposition process. Since the sputter deposition is an atomistic process, the impurities are incorporated into the structure of the coating, which may change its properties significantly [28, 29]. Ideally, the trace amounts of impurities have a negligible effect on the properties, which favors the robust deposition process and eases production.

1.5 Research experimental details and technical aspects

The author's doctoral research was focused on the metal-boron-carbon coatings, where the metallic component was either tungsten or tantalum. The research was conducted in collaboration with the Czech coating manufacturer SHM, s.r.o. on the industrial deposition system. The system was provided to Masaryk University for the purpose of this research. Figure 1.5 shows the schematic of the system. Main body creates the high-vacuum chamber with internal dimensions $550 \times 550 \times 850$ mm evacuated by the turbomolecular vacuum pump backed with rotary oil pump.

The system utilizes a single sputtering source with a cylindrical target, which can be placed in the chamber's center or in the door. The substrates are mounted to holders on the rotating planetary table (carousel) and are capable of 2-axis rotation, see the schematic in figure 1.5b. The carousel and substrates are isolated from the chamber and connected to voltage power supply so a bias potential can be applied during deposition. Resistive heating elements are placed on the inner walls to heat the chamber and substrates radiatively.

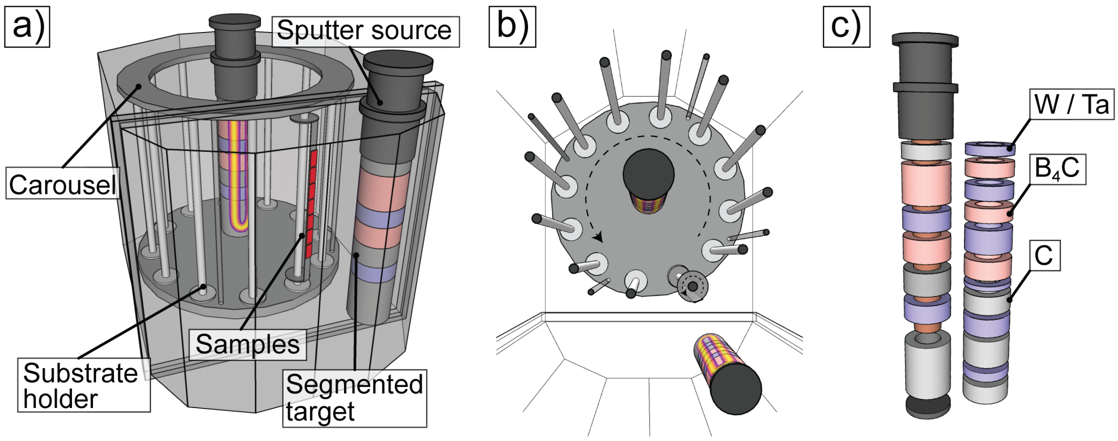

Figure 1.5: Schematic model of sputtering system utilized for the research, a) overview, b) top view, and c) sputter source with the segmented target and alternative setup.

The software fully controls the deposition process, which has been adapted to provide manual and semi-automatic control modes while ensuring all safety features are maintained. The software provides process parameter logging with a one-second step from sensors and units, including pressure gauges, mass flow meters, thermocouples, power supplies, etc. The operator controls all parameters in manual control mode, and their changes are executed instantly. The semi-automatic mode provides the ability to gradually change the parameter value in a given time interval, which can be used, for example, during power ramp-up.

The developed deposition process is based on the non-reactive dcMS of the segmented target in the argon atmosphere. The sputter source with segmented target shown in figure 1.5c is chosen to increase the flexibility of the research. The target comprises metal segments, boron carbide segments, and carbon segments. The segments' size and placements control the coating's chemical composition. Unlike the compound target, the segmented target enables adjustment of the coating composition without synthesizing a new target, which highly reduces the research cost. The table 1.2 summarizes important details and process parameters and their value range attainable with this particular sputtering system.

Parameter	Value
Base pressure	$< 5 \cdot 10^{-3}$ Pa
Working gas	argon
Working pressure	0.10 – 5 Pa
Temperature	ambient – 550°C
Substrate:	
bias potential	0 – 1000 V
motion	1-axis or 2-axis rotation
rate	0 – 12 rpm of carousel
Sputter source:	
method	dcMS
input power	0.2 – 25 kW
target type	cylindrical ($\varnothing$100 mm $\times$ 420 mm)
target material	segments of B_4C, C , W or Ta

Table 1.2: Details of sputtering system and deposition process parameters.

A combinatorial approach was utilized to deposit coatings of different compositions. It enabled to deposit multiple samples of different stoichiometries in one batch, which is ideal for studying the influence of coatings' chemical composition because deposition process parameters are identical in principle. Usually, the combinatorial approach is performed utilizing multiple sputter sources with different targets. Samples closer to the given target exhibit a higher concentration of this target material. The combinatorial approach with a single cylindrical segmented target can be achieved by rearranging the segments to attain the chemical composition gradient along the vertical axis. It thus allows to employ standard substrate motion utilized in the batch-coater. The examples of two different target setups are shown in figure 1.5c. Both are designed to capture the evolution of the boron to carbon ratio, but at different amounts of the metal constituent in the coating. The setup on the right-hand side provides a higher concentration of metal in the coating than the left one.

1.6 Inherent multilayering of coatings

The batch-coaters are often distinct from the laboratory machines by the substrate movement during the deposition process, creating another industrial research challenge. The substrate is in motion during the deposition to ensure uniform coating and increase batch size.

The substrate motion influences the deposition process and coating properties. It was reported that employing multiple sputter sources or reactive processes with the combination of substrate rotation can cause periodic modulation of the growth conditions during deposition [30, 31], which consequently leads to either intentional or unintentional preparation of multilayered coatings. However, multilayering may be present even when utilizing a single sputter source and a non-reactive process. Such effect of substrate motion was previously unknown and was discussed in the author's paper 4.1, which described this in the case of industrially deposited W-B-C coating.

A feasibility study of W-B-C coatings deposition from the segmented target was conducted during the initial phase of the author's doctoral research, and thus many coatings were prepared under various deposition conditions. Routine imaging of the coating's cross-section by scanning electron microscopy (SEM) showed rather unexpected features. Coatings exhibited multilayered structure visible on the cross-sectional SEM images as a set of bright and dark layers. However, the thickness and count of the dark and bright double layers were not identical for coatings from single deposition batch.

The multilayering pointed to periodic changes in deposition conditions during the growth of the coating. Since deposition process parameters were kept constant during the depositions and no monitored parameter exhibited any periodical changes, the origin of the multilayering was unknown. However, the substrates performed a 2-axis rotational motion which is a type of periodic cycle in some sense.

The 2-axis motion consisted of revolution around the central axis of the carousel and rotation around the substrate holder coupled through gears. The motion of the substrate holders was recorded using time-lapse footage, effectively capturing the position of the sample after each revolution of the carousel. The processed footage showed that each substrate holder performed slightly different motion, which clarified the different multilayering within a single deposition batch. Consequently, the coating growth was influenced by the choice of the substrate holder, which was a design flaw. It was a consequence of gear ratios and a lack of locking pins that prevented the slipping of the substrate holders.

Addressing this design flaw was possible to study the substrate motion in a more controlled experiment. For the purpose of the publication 4.1 were utilized three types of substrate motion (schematic available in Fig. 3 of publication 4.1):

1-axis rotation – substrate revolves around the carousel's central axis

2-axis rotation – substrate simultaneously revolves around the carousel's central axis and around holder's axis, two sub-types were distinguished:

- random – after single revolution, substrate is in apparently random position
- gradual – after single revolution, substrate is turned by a few degrees

Each motion type exhibited a distinct cross-sectional pattern of the coating imaged by SEM, see the images in figure 1.6a (top row). The cross-sectional SEM images of the 1-axis rotation samples showed no multilayering, and both types of 2-axis rotation (random and gradual) showed different multilayers.

The bright and dark layers were initially observed using the detector for secondary electrons. Their contrast was improved by switching to the signal from back-scattered electrons, which pointed to the compositional difference between the dark and bright layers. Although the chemical analysis using energy dispersive spectroscopy on the electron microscope showed the differing composition of the layers, the cross-sectional analysis was problematic and did not provide the required resolution. Therefore, the GD-OES analysis (glow discharge - optical emission spectroscopy) was performed on the samples. This technique enabled depth profiling of the sample, measuring the intensities of boron, carbon,

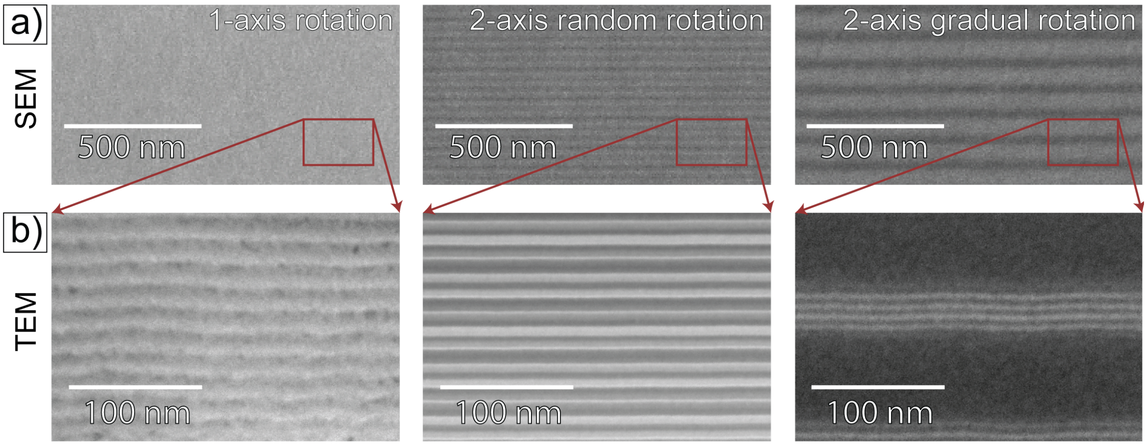

Figure 1.6: The multilayered structure formed within the W-B-C coatings visualized by a) scanning electron microscopy and b) transmission electron microscopy.

and tungsten emission lines and correlating them with the composition. The analysis revealed the periodic change of boron, carbon, and tungsten content, which corresponded to the count and thickness of the layers. The modulation in boron and carbon content was opposite to the tungsten content.

To investigate the multilayers in more detail, the transmission electron microscopy was performed on the samples. The analysis confirmed the layering, but it revealed an even finer structure shown in figure 1.6b (bottom row). Each sample exhibited layering with the thickness of several nanometers due to modulation in the composition.

Considering the thickness of the coating and the total count of revolutions that the substrate performed during the deposition, it was possible to derive the thickness increment of the coating per one revolution. It matched the thickness of the fine double layers.

The multilayers were, thus, unambiguously connected to the substrate motion and were a fingerprint of compositional modulation in the coating. When the rotation was disengaged, the composition of the coating was a function of the position within the chamber. The hypothesis was that the particles follow different pathways due to scattering on the working gas atoms. During sputtering, the particles must undergo several collisions with atoms of working gas to reach the substrate. In the hard sphere approximation, the scattering angle is a function of the reduced mass of the two bodies. The boron and carbon atoms are prone to high-angle scattering due to low mass relative to the argon atoms. On the other hand, the heavy tungsten atoms are more likely to stay on the direct pathway.

The conclusions from publication 4.1 influenced the following research significantly. After modifying the planetary table and holders, each holder performed an identical motion, and the design flaw was therefore fixed. The substrate motion was carefully monitored, and rotation speed was marked as an important deposition parameter because it controls the double layer thickness. The multilayered structure was always expected to be present if the substrate was in motion during the deposition.

Chapter 2

Me-B-C coatings

As indicated by the name itself, the hard protective coatings' main feature is their high hardness, i.e., resistance to localized plastic deformation. If applied on the tool's cutting edge, it provides the ability to cut through a wide range of materials but simultaneously, the hard surface with good adhesion to the substrate is wear-resistant and increases the tool's lifespan. The coated tools withstand high temperatures, oxidation, and corrosion and provide low friction [32]. Apart from the cutting tools, the coating is routinely applied on dies and molds and is used for many other applications where mechanical and thermal fatigue or wear occur.

Common coating materials are listed in table 2.1 with reference values of mechanical parameters and oxidation stability, noting the reported values range significantly depending on the deposition process, and other factors [33]. The first generation of hard protective coatings was based on metal nitride ceramics because they provided the stiffness necessary for high surface hardness. The nitrides exhibited various properties depending on the nitride forming element and the structure of the resulting material.

The nitrides of transition metals from groups 4-6 of periodic table were common because they exhibited higher hardness than uncoated high-speed steel tools ($\sim$10 GPa) and cemented carbide tools ($\sim$15 GPa). Unambiguously, the most established was the titanium nitride. With appealing gold color and hardness about $\sim$25 GPa, the TiN coating quickly gathered popularity on tools and for optical applications or decorative purposes. Utilizing other transition metals like Cr, Zr, Ta, and others affected the appearance and mechanical properties of the resulting coating.

The hard nitride coatings are not limited to transition metals only. For example, the AlN coating electrically insulates but provides high thermal conductance; the cubic-BN excels with hardness, and the Si_3N_4 combines high hardness with good chemical resistance [33].

While the binary nitrides are still popular and often used as standard coatings for a wide variety of applications, the ternary nitrides TiAlN and AlCrN have continuously replaced them in many applications. They are metastable solid solutions that exhibit high oxidation stability due to the layer of dense protective oxides formed on their surface in oxidative environments. The oxidation onset is around 800°C, which is a substantial improvement compared to the originally used TiN [17, 38].

The carbides are similar to the nitrides in terms of their structure and properties, but they

Material	H (GPa)	E (GPa)	B (GPa)	G (GPa)	B/G	T_{ox} (°C)
TiN	25	514	295	213	1.39	450
ZrN	20	377	250	151	1.66	550
AlN	13	486	280	190	1.47	800
cubic-BN	50	450	376	384	0.98	850
TiAlN	31	395	280	210	1.33	800
AlCrN	25	375	250	188	1.33	1000
TiC	30	440	250	181	1.38	400
TiB_2	40	480	238	240	0.99	1000

Note: H – hardness, E – Young modulus, B – bulk modulus, G – shear modulus, T_{ox} – oxidation temperature

Table 2.1: Common materials utilized as hard protective coatings [33–40].

usually exhibit higher hardness compared to corresponding nitrides [38]. The deposition of carbides is usually more challenging to attain as it often involves a reactive process based on hydrocarbon gasses, which are far more complex. The TiC coating is commonly offered because it delivers mechanical properties that can be tailored, ranging from the superhard coatings (hardness $>$ 40 GPa) to coatings with very low friction coefficient only by changing process parameters [41].

The borides generally exhibit the highest hardness and modulus when compared to nitrides and carbides of transition metals because the covalent boron-boron bonds has higher strength than the bonds in the structure of the nitrides or carbides. The sputtered TiB_2 provides outstanding hardness and excels in oxidation stability, and chemical resistance [33, 38].

Although these ceramic-based materials usually excel with hardness, their common drawback is brittleness, i.e., they tend to form and spread cracks. When subject to stress, the materials fracture rather than deform, which for coatings on tools means failure, immediate loss of the protective properties, and potential damage to the tool and the workpiece. Chasing the highest hardness values in the pursuit of finding the superhard material is thus not necessarily the ideal approach for protecting tools' surfaces.

According to Pugh [42], the metals' brittle/ductile behavior is correlated to the ratio of bulk to shear modulus B/G. The higher the ratio, the more ductile metal. The so-called Pugh criterion has been adopted for various pure and compound materials. In literature, the value $B/G = 1.75$ is commonly agreed as the deciding point on which the material is either brittle or ductile. It must be noted, though, that the 1.75 value is a vague generalization of the criterion and must be understood as indicative only. In Pugh's original analysis, the specific value of B/G was not proposed because the actual critical value depends on the material's elastic anisotropy and, according to Senkov et al., ranges for cubic crystal structures between 1.66 and 2.38 [43].

Applying the Pugh criterion on the hard protective coatings from table 2.1, the B/G suggests all of the coating exhibit brittle behavior. And in fact, this corresponds to the experimental experience. Upon the indentation tests, these coatings exhibit cracking and chipping [44]. From industrial experiences, it is well known that during use, the instant failure of these coatings is imminent, which resembles the fracture of ceramic bulk [45].

Nanostructuring Nowadays, the material design has advanced beyond the single phase coatings, and the structure is tuned on a nanoscopic scale, improving mechanical properties. A common approach is to utilize heterogeneous structuring that combines materials with different mechanical properties, e.g., hard brittle with soft ductile. As a result, the hardness and elastic modulus may improve, and the propagation of cracks and formation of dislocations is more difficult as well, which decreases the probability of instant failure of the coating.

The *nanocomposite coatings* benefit from crystalline grains with a size of a few nanometers embedded in the amorphous matrix. The small size of the grains limits the dislocation formation, and the cracks are less likely to propagate through the grains and would have to change the direction of propagation multiple times to evade the grains. This consequently lowers the probability of the crack spreading.

The *nanolayering* of mechanically different materials adds many interfaces to the structure, on which the crack may deflect as it is less likely to propagate through the soft ductile material and thus, the crack spreading is again limited.

The *functionally graded coatings* are based on composition gradient. Their properties gradually vary along one spatial coordinate (usually along the growth direction), which limits the crack propagation through the thickness of the coating, and it likely stops in its volume.

Because the nanostructuring removed some drawbacks of the single phase coatings and provided better mechanical properties [46], the industry adopted these approaches, and their top-shelf coatings usually combine multiple materials and utilize the aforementioned structures, and their combinations [47]. Still, the hard materials are primarily based on brittle ceramics, which consequently limit the coatings' performance.

The coatings composed of metal, boron, and carbon (Me-B-C) have the potential to address the common brittle nature of the hard protective coatings and advance this field further. The Me-B-C materials are studied with potential application as hard protective coatings for tools. Even though many materials are now routinely deposited as hard protective coatings, the Me-B-C materials introduce beneficial features for the coatings. The focus on the Me-B-C coatings started in 2009 following the work of prof. J. M. Schneider's research group from RWTH Aachen in Germany. On the basis of calculations and experimental work, their study proposed the orthorhombic Mo_2BC phase as a material suitable for hard protective coatings [34] as it provides a combination of stiffness and moderate ductility.

2.1 Proposal of Me_2BC crystalline phases

The research of metal-boron-carbon coatings was initially focused on one particular ternary crystalline phase with the general composition of two metal atoms per carbon and boron atom – Me_2BC. The unit cell of the Me_2BC phase exhibits orthorhombic crystal structure with Cmcm (63) space group and was first described by Jeitschko et al. [48] in 1963. The study presented and proved the molybdenum-based Mo_2BC crystalline phase, see the original drawing in figure 2.1. The cell consists of Mo_6B layers separated by the Mo_6C

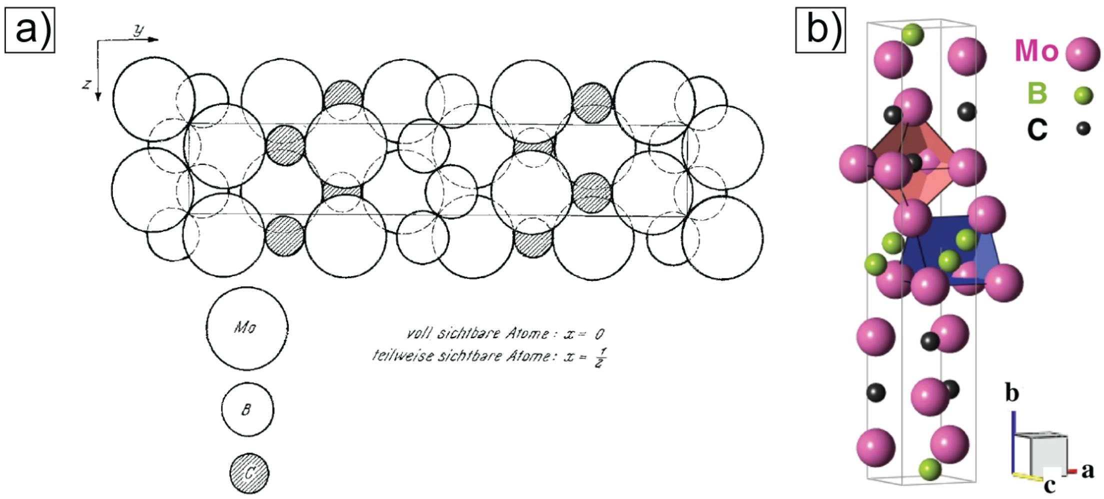

Figure 2.1: a) The original drawing of the Mo_2BC unit cell by Jeitschko et al. [48] and b) the visualization of the Mo_2BC unit cell from [34].

layers [34, 49]. The orthorhombic Mo_2BC phase was synthesized in a single crystal form by congruent melting and identified from the x-ray reflections.

Even though the bulk Mo_2BC was studied for its superconducting properties [50], the mechanical properties were mostly overlooked. The focus on the mechanical properties and specifically on the properties of the Mo_2BC thin film was initiated much later. Emmerlich et al. noticed similarities of the Mo_2BC structure with MAX phases[1], which often exhibit higher ductility while still preserving the stiffness [52]. They performed calculations based on the density functional theory (DFT) and derived elastic constants of the Mo_2BC phase from which the elastic moduli and Poisson ratio were determined. It showed the value of $B/G = 1.73$, which suggested moderately ductile behavior. Within the study, they also synthesized the Mo_2BC in the form of thin film by magnetron sputtering and presented its properties that corroborated with the theoretical predictions.

Later Bolvardi et al. [35] conducted a systematic theoretical study of multiple materials with identical phases utilizing the same ab-initio approach. The molybdenum was replaced by other transition metals, and a total of seven phases of Me_2BC-type structures were assumed as proposed in [48]. The calculations showed that the enthalpy of formation of every material was negative (see table 2.2), which suggests all the phases were stable and could exist. The elastic moduli were dependent on the metallic component.

Table 2.2 sorts the materials according to B/G ratio. The first three places take the phases with tungsten, molybdenum, and tantalum. These phases have comparable bulk modulus to state-of-the-art protective coatings stated in table 2.1. However, they exhibit a higher ratio of bulk to shear modulus, which points to more ductile behavior according to the Pugh criterion. The W_2BC exhibits the highest moduli and the highest B/G ratio, but the least negative enthalpy of formation suggests it is also the least stable. On the other hand, the Ta_2BC still exhibits comparable mechanical parameters to the Mo_2BC, but it

[1]Ternary carbides or nitrides of transition metal and element from group 13-15 of periodic table with general formula $M_{n+1}AX_n, n = 1,2,3$ and layered unit cell composed of MX and A layers (M: transition metal, A: element from group 13-15, X: nitrogen or carbon) [51].

Phase	E (GPa)	B (GPa)	G (GPa)	B/G	H_F (eV/atom)
W_2BC	468	350	184	1.91	-0.161
Mo_2BC	455	313	181	1.73	-0.283
Ta_2BC	421	286	168	1.71	-0.678
Nb_2BC	404	259	163	1.59	-0.674
Ti_2BC	378	208	158	1.46	-0.891
Zr_2BC	312	187	128	1.46	-0.812
Hf_2BC	362	207	150	1.38	-0.892
V_2BC	435	260	178	1.33	-0.651

Note: E – Young modulus, B – bulk modulus, G – shear modulus, H_F – enthalphy of formation

Table 2.2: Elastic moduli and enthalpy of formation of Me_2BC phases [35].

should provide higher stability, which favors its synthesis. The W_2BC, Mo_2BC, Ta_2BC were proposed as "promising candidates for protection of cutting and forming tools" [35].

2.2 Advanced characterisation of Me-B-C coatings

Newly researched materials often come with the challenge of properly characterizing them, and the Me-B-C coatings also possess certain aspects. The specimen in the form of thin film requires specific approaches to analysis. The analytical techniques must provide sufficient depth resolution because the specimen is, in fact, a system of thin film and substrate, both often with very different properties.

Nowadays, the analytical techniques for thin films are well established. The hard protective coatings are routinely characterized in terms of their chemical composition, microstructure, morphology, and thermal or oxidation resistance, and focus is naturally given to the mechanical properties.

In the author's research, the Me-B-C coatings were analyzed with a similar focus using various analytical techniques. The focus was namely on the coatings' growth, structure, and mechanical response. The employed techniques are listed in table 2.3. Combining the techniques provided a comprehensive view of the coating properties and linked them together. The selected techniques also provided spatial resolution, which was necessary when the combinatorial approach was utilized.

The analytical methods highlighted in table 2.3 are described in more detail. The following sections describe two aspects of material analysis specific to the Me-B-C coatings. Two approaches were developed for their proper characterization and assessment. The first aspect concerns the compositional analysis because the coatings are composed of elements with significantly different properties. Moreover, the coatings are deposited utilizing the combinatorial approach making the chemical composition a crucial parameter.

Another aspect lies in determining the coatings' resistance to damage and fracture upon exerting mechanical load. It is highly relevant because the Me-B-C materials are predicted to exhibit higher ductility when compared to other state-of-the-art materials used as hard protective coatings. The second approach enables to asses and compare different coatings in terms of damage resistance by adapting the instrumental indentation technique.

Imaging (surface and cross-section)	scanning electron microscopy (SEM) transmission electron microscopy (TEM) scanning TEM (STEM)
Topography	confocal microscopy SEM
Chemical composition	**energy dispersive spectroscopy (EDS)** glow discharge optical emission spectroscopy (GD-OES)
Thickness	calo-test + confocal microscopy cross-sectional imaging (SEM)
Microstructure	x-ray diffraction (XRD) selected area electron diffraction (SEAD)
Internal stress	3D profilometry
Hardness Elastic modulus Damage resistance	**instrumental indentation**

Table 2.3: List of analytical techniques utilized for the characterization of W-B-C and Ta-B-C coatings. Highlighted techniques were adapted to serve for proper characterization of the Me-B-C coatings.

2.2.1 Standard-based energy dispersive spectroscopy

The composition analysis is highly suggested when researching sputter-deposited coatings because its stoichiometry depends on several factors. When utilizing the co-sputtering of multiple materials, the composition depends on the power delivered to the individual target, the sputtering yield of the material, and the distance of substrates to individual targets.

Even though the parameters of targets are usually very accurately predetermined by the manufacturer and the composition of the coating is closely related to the target composition, it may not always match it. During the transport some sputtered particles are lost on the chamber walls and do not reach the substrate. If the rate of particle loss is element-dependent, the coating composition differs from the target composition.

Effects connected to ion bombardment of growing coating or reactive processes also take place during sputtering making it hard to estimate the resulting composition of the coating. The composition of the coating must be thus determined by analytical methods. One of the most applied and broadly available method is energy dispersive spectroscopy (EDS), which enables fast elemental microanalysis and chemical characterization.

The EDS uses a beam of primary electrons accelerated to an energy of several keV to obtain analytical information. It is based on electron-excited characteristic x-ray radiation that originates from the specimen when the primary electron displaces an electron from the atom's inner shell. Depending on the electron energy, specimen density, and material's x-ray absorbance, the characteristic radiation is acquired from a volume around 0.5-5 μm deep under the specimen surface [53], which makes it suitable for the analysis of thin films.

The EDS often serves for the qualitative and quantitative x-ray microanalysis in scanning electron microscopes (SEM), thus providing good spatial resolution as well. A detector mounted to the SEM acquires the x-ray radiation and records the EDS spectrum, i.e., the dependence of x-ray intensity on its energy. Elements are identified from the position of peaks in spectra. The quantitative analysis is based on the intensity of the x-ray radiation.

The Me-B-C coatings, specifically those with tantalum and tungsten, are composed of elements with substantially different shell structures. The EDS spectrum thus combines x-rays radiation corresponding to transitions to K, L, M, and N shells. Figure 2.2 shows the EDS spectrum of sputter deposited W_2BC and Ta_2BC coatings with a marked peak position of identified elements acquired at 8 kV of electron accelerating voltage.

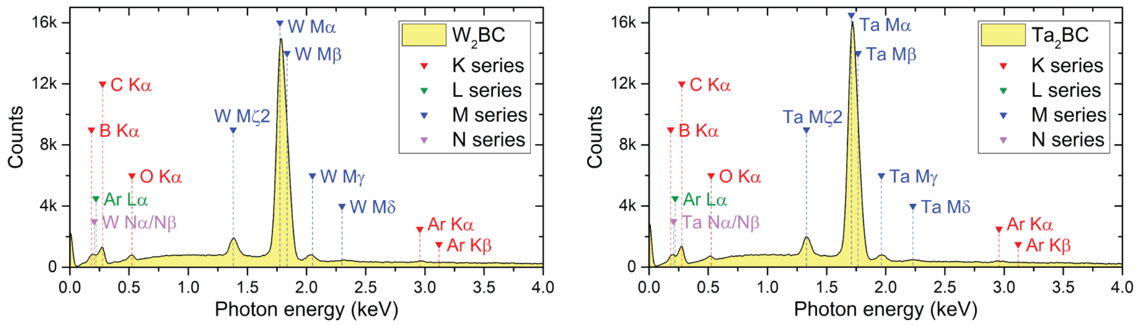

Figure 2.2: Energy dispersive spectra of sputter deposited coatings with composition W_2BC and Ta_2BC acquired with electrons accelerated to 8 keV.

The boron, carbon, and tungsten/tantalum are the main constituents of the coating, a small amount of argon is incorporated in the coating structure during the deposition process, and oxygen is a surface contaminant after exposing the specimen to air. The spectrum exhibits interference on the low energy side. The K_α lines of boron and carbon located at 0.18 keV and 0.28 keV, respectively, are separated only by 0.10 keV. And the Ar L line and N lines of metals are also observed in near vicinity at ≈ 0.25 keV.

Processing of the spectra is usually performed within the acquisition software for the EDS probe, e.g., AZtec for probes manufactured by Oxford Instruments [54] or ESPRIT for Bruker probes [55]. The analysis is performed through an internal library of standards provided with the software and bound to the specifics of the detector and its placement relative to the beam and specimen. Other software like NIST-DTSA II [56] that provides advanced control of the spectra processing is also available, but it requires extensive knowledge about the detector, spectrum acquisition, and quantification process.

The quantification is based on the previously acquired standards. Most often, the standards are single elements or binary compounds, which is not ideal for the Me-B-C coatings. The x-ray attenuation coefficients of tungsten and tantalum are an order of magnitude higher than for boron or carbon [57], which results in the underestimation of boron and carbon content in the Me-B-C coatings when the standards do not contain all three elements. Moreover, the interference of the boron and carbon K_α lines and metal N line makes it difficult to determine the ratio between boron and carbon content.

Processing software often enables editing the standards library and introducing additional materials. However, providing a standard that is *most alike* to the analyzed specimen is crucial. Such standards may be obtained with little effort in the PVD laboratory and quantitative analysis can be performed as described by figure 2.3.

The first option is to use bulk material with known chemical composition that contains the elements of interest, for example, synthesized by alloying or from hot pressed powders by sintering. Such materials can be found conveniently in the PVD laboratory as the sputtering targets after their lifetime. Since the manufacturing procedure inherently guarantees the composition of the target, the nominal composition used for quantification is very precise. However, the analysis may struggle with the differences in structure and morphology between the standard and unknown sample.

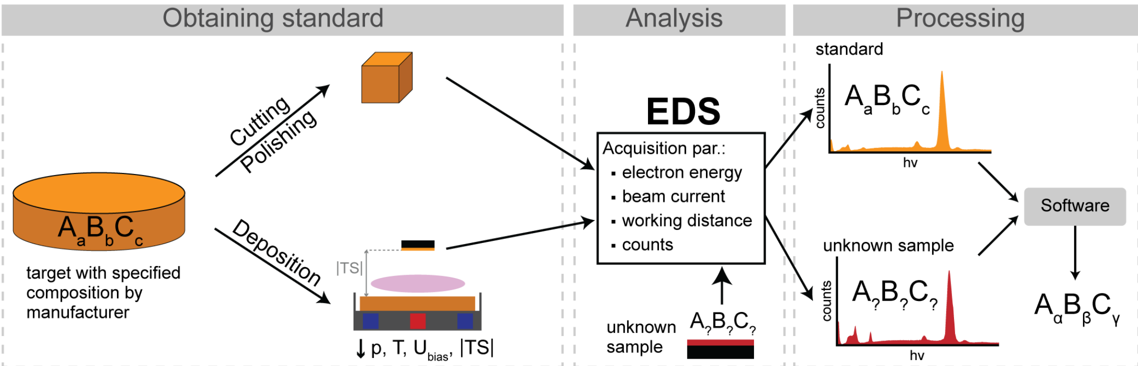

Figure 2.3: Schematic of standard based EDS analysis.

The second option is to use sputter deposited coating from the compound target as the standard, provided the composition of the coating can be assumed to match the composition of the target. Sputtering ensures that in steady-state, the composition of the coating is the same as the target if all particles are deposited on the substrate and their loss due to scattering and other effects are negligible or at least element independent [58]. The best approach is to mount the substrate close to the target, lower working gas pressure to increase the mean free path, and disable the substrate biasing and heating. After that, the composition of the deposited coating can be assumed to be identical to the target. This method is beneficial because the standard is prepared on an identical substrate, and the resulting structure is similar to the unknown specimen.

If and only if the EDS spectrum of such standard is acquired under identical conditions as the unknown specimen, i.e., accelerating voltage, beam current, working distance, and the total number of counts, the spectrum may be used to standardize the quantitative analysis. If performed properly, the standard-based EDS enables quantitative analysis with high accuracy, and precision [59]. Table 2.4 summarizes details of the analysis used for Ta-B-C and W-B-C coatings.

Acquisition	
Electron energy	8 keV
Beam current	~1.1 nA
Working distance	15 mm
Counts	500 000 (constant)
Acquisition area	50×50 µm

Standardization	
Standard type	sputtered coating
Standard composition	W_2BC, Ta_2BC
Intensity calibration	silicon (100)

Table 2.4: Details of EDS analysis for W-B-C and Ta-B-C coatings.

2.2.2 Estimating coatings' resistance to damage and fracture

Demands dictate to develop a hard protective coating that would withstand damage and be less likely to fracture. Several approaches exist to evaluate this property, but these were initially developed for bulk materials. In essence, the stress-strain behavior is studied, which describes how the materials withstand mechanical stresses. During the loading, the energy is deposited in the material, and the induced mechanical stress causes strain, corresponding to the elastic deformation, plastic deformation, and formation of cracks that propagate through the material and consequently cause a fracture.

Strong ductile materials absorb a high amount of energy and exhibit extensive plastic deformation before fracture. Strong brittle materials, on the other hand, absorb less energy, and the fracture may occur without the deformation. The quantitative measure of cracking is the fracture toughness which indicates the critical stress intensity for the propagation of a pre-existing crack. Depending on the direction of crack propagation and stress field, three cracking modes can be distinguished – opening, sliding, and shearing mode, see figure 2.4, each connected to individual fracture toughness K_{Ic}, K_{IIc} and K_{IIIc}, respectively. Arbitrary load on the crack is a combination of these three modes [60].

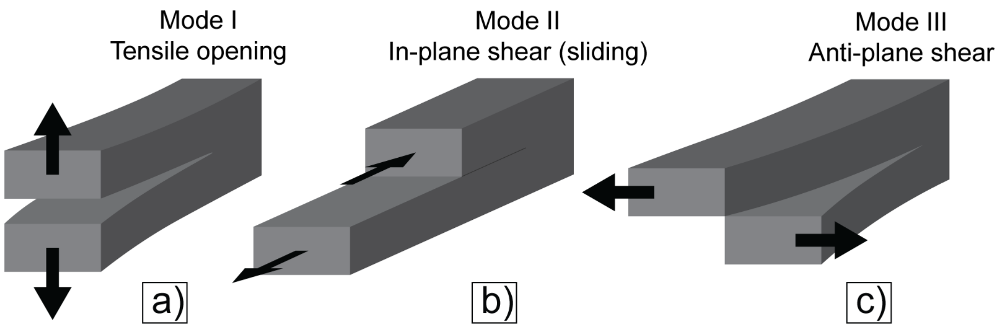

Figure 2.4: Cracking modes: a) Mode I – opening, b) Mode II – sliding, c) Mode III – shearing. Schematic redrawn according to [61].

Empirical criteria Estimates about materials' brittle/ductile behavior can be assessed by empirical criteria. The Pugh criterion based on the B/G ratio is often used in conjunction with the Pettifor criterion, which is based on quantum mechanical analysis [62]. It states that ductility is related to the difference between elastic constants $c_{12} - c_{44}$, the so-called Cauchy pressure. The positive Cauchy pressure shall indicate the non-directional metallic bonding and, thus, intrinsic ductile behavior of the material. The Pugh and Pettifor criteria are mainly used to predict the behavior of theoretically researched materials [43, 62].

Experimentally, the toughness of bulk materials is tested by bending, tensioning, or shearing. Evaluating the strain-stress behavior for coatings is more challenging because it is a system of thin film and substrate. The analytical technique is thus required either to operate with a very small volume of material or account for the substrate effects. Material scientists adopted several methods in a number of studies to evaluate the coating properties.

The H/E and H^3/E^2 ratios are often utilized as measures of fracture toughness and resilience for coatings because hardness and elastic modulus are conveniently derived from routine analysis of mechanical properties by indentation test. The empirical rule states, the higher values of these ratios, the higher fracture toughness and wear resistance of the coating. Such correlations were shown in several studies of nanocomposite coatings [63–65]. However, if the coating fracture involves plasticity and does not exhibit instant failure, the ratios showed inverse or no correlation with the fracture toughness, making the method not generally applicable [66].

Indentation-induced cracking A widely applied method for evaluating fracture toughness is indentation-induced cracking. It is based on applying sufficient load through a sharp indenter tip to induce the formation and spreading of cracks in the material. It relies on direct measurement of the radial cracks emerging from the corners of the indentation imprint. Figure 2.5a shows indentation-induced cracking of 0.6 µm thick TiN coating on a silicon substrate. The length of cracks is measured in plane view to prevent error readout due to image distortion.

Since the length of cracks was shown empirically related to the fracture toughness, several models to evaluate the K_{Ic} were developed. Depending on the morphology of cracks and material type, a suitable model needs to be chosen, and fracture toughness is calculated from the crack length, hardness, and elastic modulus of the material [67–69]. Even though the calculation utilizes an arbitrary constant related to the material, the geometry of the indenter, and crack morphology, the method proved well for bulk materials and is often used for coatings [70, 71].

However, caution must be exercised when utilizing this method for sputter deposited coatings. The models assume fully developed cracks, i.e., crack is much longer than the diagonal size of the imprint, and given the type of the geometry of the crack system [67–69, 76]. The state-of-the-art coating often cannot comply with these presumptions, and the choice of the proper model can be extremely challenging in practical cases. Moreover, the sputter-deposited coatings often exhibit internal stress, which causes the closing of the cracks to the extent that they are not sometimes visible. Consequently, this leads to overestimating the resulting fracture toughness [71, 77].

Micro-scale testing structures When focused ion beam (FIB) milling became more available, new techniques of fracture toughness measurement were developed. The FIB enabled in-situ micro-machining of the specimen with great precision. The size of milled details is in the nanometer scale. It is possible to fabricate cantilevers, pillars, and other geometries in the coating, which serves as the test structures with well-defined geometry. Combined with an instrumental indentation test or atomic force microscope, it is possible to measure the mechanical response of such specimens to the applied load.

An example of a cantilever is shown in figure 2.5b. The FIB is used to undercut the coating and create a beam with a free end. The load is applied through the indenter tip close to the free end, which causes bending, elastic deformation, and subsequent fracture. To provide repeatable and defined fracture, the so-called pre-notch is milled at the base of the cantilever. Upon loading, it fractures along the notch, which enables to calculate the K_{Ic} according to the empirical model for the given geometry of the cantilever [72].

A micro-pillar milled from the coating is shown in figure 2.5c. Testing is carried out either by splitting [74] or by compression [75]. In case of splitting, the pillar is loaded at

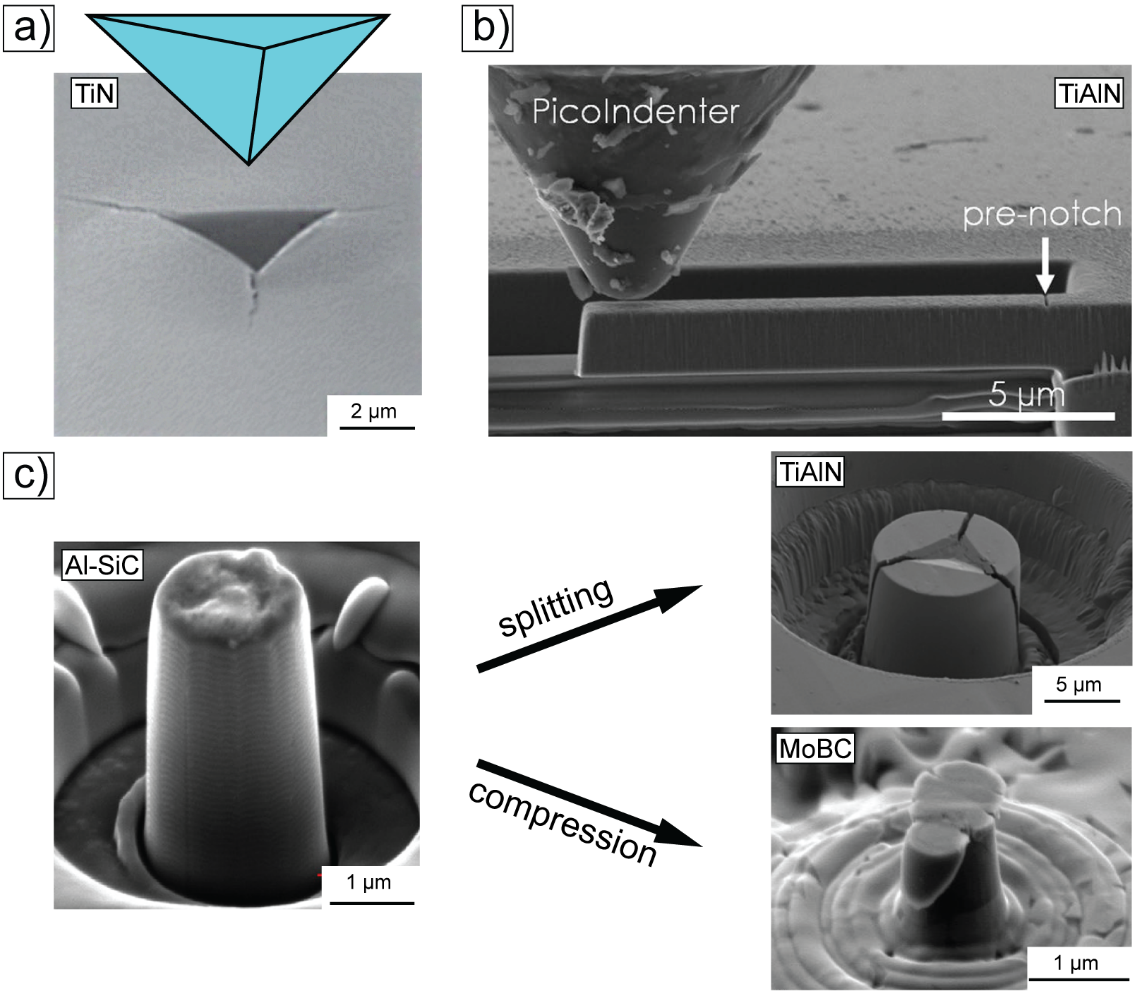

Figure 2.5: SEM images of a) induced cracking of TiN after indentation test [44] b) in-situ cantilever bending test [72] c) micro pillar prior and after splitting and compression tests [73–75]. Size and labels of images are adapted.

the top center by a sharp indenter to produce cracks that split open the pillars into three parts, ideally of equal size. The calculated fracture toughness then becomes independent of the crack length, which is the main advantage of this method [72]. The micro pillar compression method is performed by swapping the sharp indenter for a flat punch indenter, which provides uniaxial and uniform load on the pillar to evaluate the stress-strain behavior [73]. The goal is not to generate defined cracking but to obtain a stress-strain curve and evaluate the pillar after breakage. The uniaxial stress causes compression of the pillar and may reveal dislocation slips and shear or kink bands.

The micro-scale toughness evaluation is still a relatively new technique, and it yet lacks well-established standards for the specimen geometries and measurement procedures. The effects of the FIB milling on the material properties are also yet to be profoundly described. The ion irradiation of the specimen may cause unavoidable altering of microstructure as it induces an amorphous layer on the specimen surface and implants ions into its structure. Depending on the utilized system, it may alter the specimen's mechanical properties to a greater or lesser extent [78].

Damage parameter The predicted tough yet ductile Me-B-C materials make it very difficult to utilize any method based on cracking due to the lack of pure brittle fracture. In order to evaluate their resilience and compare them to very different types of coatings, the evaluation method must cover a wide range of possible damage and fractures caused by mechanical stress.

According to Zeng et al. [79], the damage that material sustained during the indentation test is correlated to the elastic modulus. The cracking and damage make material locally more complaint. Thus the elastic modulus of damaged or cracked material – so-called damage modulus E_D is lower than the unaffected modulus E. The relative change of these provides a damage parameter $D = 1 - E_D/E$, which evaluates the severity of the damage that material sustained [79]. The higher the damage parameter, the more severe the damage.

Since the method is based on the elastic response of the induced damage, it considers every fracture mode. The method thus can be utilized even if the material exhibits no visible cracking and develops deformation during indentation tests differently. It can exhibit shear bands, slip planes, voids under the surface, etc., which is often the case with ductile materials. The damage parameter was utilized for the ceramic, glass, and composite bulk materials [79], but seemingly, the method may be adapted for the coatings as well if some precautions are made.

The indentation test is performed at multiple maximal loads to calculate the damage parameter. Low loads provide the unaffected elastic modulus. High loads provide the damage modulus if any damage is induced.

Figure 2.6 demonstrates an example of the damage parameter evaluation. The tungsten and fused silica bulks were chosen here because of their different fracture toughness. Compared to fused silica ($K_{Ic} \sim 0.6\,\mathrm{MPa}\sqrt{\mathrm{m}}$), the fracture toughness of tungsten is reported in the literature as significantly higher ($K_{Ic} \sim 6.5\,\mathrm{MPa}\sqrt{\mathrm{m}}$) [80, 81]. The damage parameter is derived from evolution of the elastic modulus as a function of applied load.

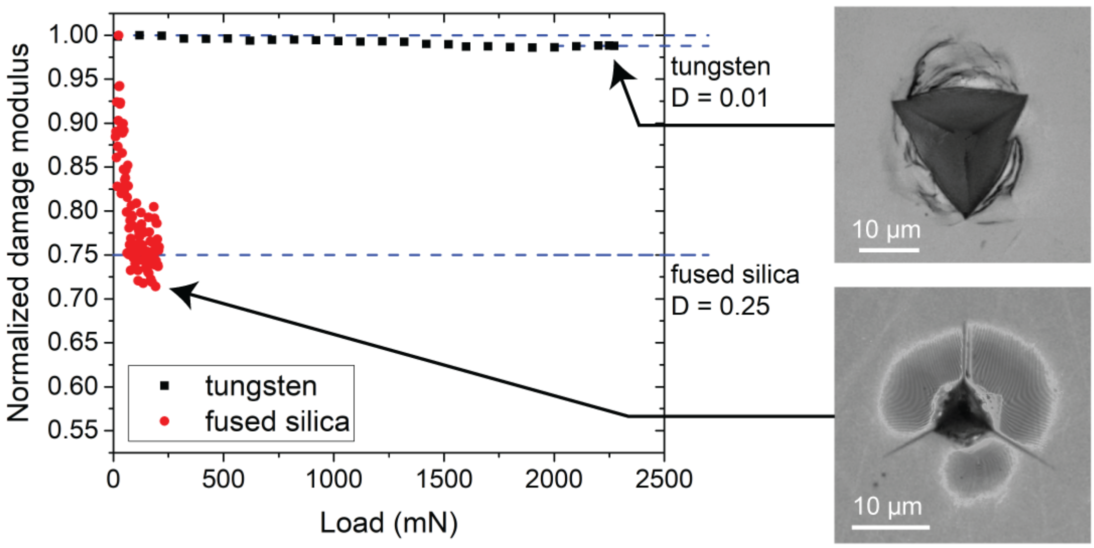

Figure 2.6: Damage parameter evaluation for tungsten and fused silica. Insets show residual indentation imprints taken by confocal microscope.

The elastic modulus of the tungsten and fused silica exhibited significantly different evolution. The tungsten exhibits a minor decrease in the modulus, and the resulting damage parameter is close to 0. On the other hand, the fused silica exhibits a significant decrease in the modulus, and the damage parameter is 0.25. The confocal images confirm that damage of tungsten is negligible, while significant cracking is observed on the fused silica. The cracks emerge from the corners of the imprint, and simultaneously lateral cracks are present under the imprint (indicated by the interference fringes around the imprint). The damage parameter, therefore, can describe the severity of the induced damage and compare the materials in terms of their brittle/ductile behavior.

However, in the case of coating, the coating-substrate interface may interfere with the measurement as the deformation zone reaches the interface, and the mechanical response is a superposition of the coating and substrate properties. This often results in apparently lower elastic modulus, even for undamaged coating. To derive the damage parameter correctly, it is required to induce damage during the high load measurement while limiting the interference of the coating-substrate interface and substrate itself.

While the Berkovich and Vickers indenters with semi-angles of 65.3° and 68.0°, respectively, are utilized for routine analysis of hardness and elastic modulus of coatings, the sharper cube-corner indenter with smaller semi-angle (35.6°) is more suitable for damage parameter method. The cube-corner indenter displaces more material compared to Berkovich and Vickers at the same indentation depth. Consequently, it induces a higher local concentration of stresses with a smaller deformation zone [82]. The damage parameter for coatings thus can be derived from an indentation test utilizing a cube-corner indenter. Noting the large thickness of the coating is highly beneficial to ensure that the effect of the coating-substrate interface is negligible.

The derived damage parameter is then assessed in combination with an analysis of the load-displacement curves and imaging of the residual imprints to provide a comprehensive analysis of the sustained damage.

2.3 State of the experimental research of Me-B-C coatings

Research groups have studied the Me-B-C coatings focusing on the orthorhombic crystalline phase since 2009. Upon now, in November 2022, the only successfully synthesized phase is Mo_2BC, and no strong proof of other phases has been found. Even so, the lack of the orthorhombic phase may not be a drawback because the metal boron carbide coatings exhibit promising properties even without any crystalline phase presence.

Most experimental works were focused on the molybdenum based coatings, but systems with tungsten, tantalum, niobium, and titanium were also studied. See the timeline in figure 2.7, which summarizes experimental works concerned with the Me-B-C coatings and motivated by the proposal of Emmerlich et al. [34].

In thin film form, the orthorhombic Mo_2BC in 2009 was first synthesized by magnetron sputtering in Aachen, Germany [34]. Emmerlich et al. utilized co-sputtering of molybdenum, graphite, and boron carbide targets on alumina substrate heated to 900°C. The x-ray diffractogram matched the nominal reflections of Mo_2BC proving the polycrystalline orthorhombic structure of coating. The coating exhibited Young's modulus of 460 ± 21 GPa, which compares well to the predicted value from DFT calculations (table 2.2). The com-

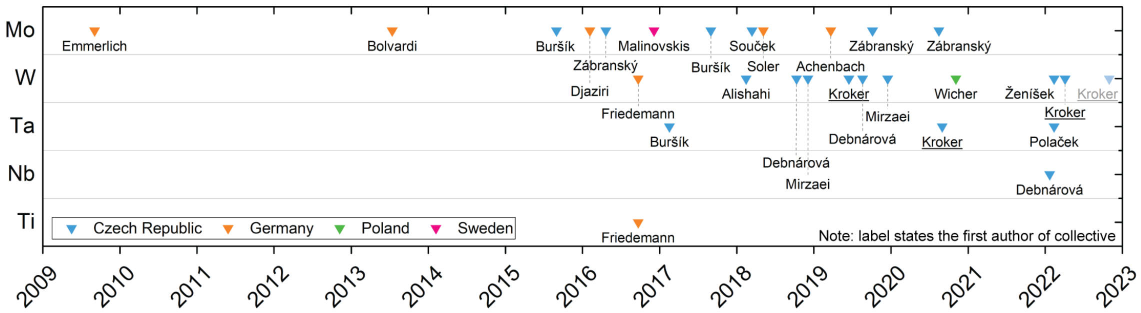

Figure 2.7: Timeline of experimental research concerned with the Me-B-C coatings focused on the Me_2BC phase. Data acquired from Web of Science [83].

bination of high hardness (29 ± 2 GPa), absence of cracking, and pile-up formed after the instrumental indentation test supported the results of ab-initio calculations and the notion that the Mo_2BC coating exhibited increased ductility while providing the high hardness.

In 2013, the Aachen research group reported the deposition of Mo_2BC phase at a lower temperature. This was possible by utilizing the HiPIMS, which increased ion bombardment of film-forming ions and argon ions, providing thus enough mobility to adatoms and increasing surface diffusion. The deposition temperature could be lowered from 820°C in dcMS case to 380°C in HiPIMS case, thus widely expanding the possible application of the coating on the technologically interesting substrates [84]. The microstructure was again presented by x-ray diffraction. The diffractograms showed two diffraction peaks, that were identified as reflections of Mo_2BC, which would correspond to highly textured structure. But, large width of the peaks suggests that the size of crystallites is small, and only the short-range ordering of atoms may be expected at lower deposition temperatures.

Increased fracture resistance of the Mo_2BC coating was later supported by Djaziri et al. After tensile stress testing, the Mo_2BC coating deposited on copper substrate showed 1.9 times smaller crack density than TiAlN benchmark coating [85]. Later, the direct measurement of K_{Ic} by microcantilever showed that the fully crystalline Mo_2BC coating exhibit the intrinsic fracture toughness of 4.5 MPa$\sqrt{m}$ [86].

While the polycrystalline Mo_2BC orthorhombic structure of coating is unambiguously beneficial, the design of the coating can be tailored further. The hardness, modulus, and stress of Mo-B-C depend on the relative amount of crystalline and amorphous phase [87–89]. Depending on the structure, the hardness of Mo-B-C coatings ranged from 20 to 28 GPa and the elastic modulus from 259 to 462 GPa. Regardless of the amount of the crystalline phase, coatings with composition around the Mo_2BC stoichiometry exhibited reduced cracking compared to TiN, AlTiN, or TiB_2 after indentation tests. If the substrate was deformed plastically without shearing, the Mo-B-C coatings complied and did not show any signs of cracking [88], see figure 2.8. It corroborates with findings that the structure has only a small influence on the intrinsic fracture toughness of Mo-B-C coating [86].

Following the predicted properties of the Me_2BC orthorhombic phases [35] and research articles being published on the Mo_2BC coatings, the interest in the Me-B-C coatings was increasing. If the goal was to benefit from the mechanical properties of the Me-B-C coating, the W-B-C and Ta-B-C systems were the next logical choice, see table 2.2.

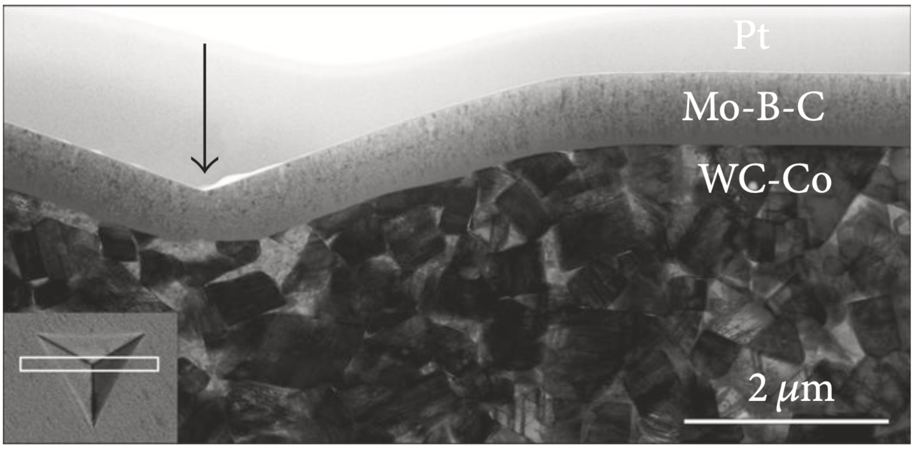

Figure 2.8: TEM of a lamella cut from a residual imprint after 1 N indentation to Mo-B-C coating. Inset shows SEM plan view of the residual indentation imprint with marked position of the prepared lamella. Image as presented in [88].

Although Friedemann et al. published first study on the tungsten- and titanium-boron-carbide coatings in 2016, the coatings were designed as boron-based, thus not approaching the Me_2BC composition [90]. The W-B-C coatings with tungsten content 12-27 at.% exhibited hardness $>$27 GPa and modulus up to 423 GPa. The Ti-B-C coatings exhibit lower hardness and modulus.

A set of studies that focused on the orthorhombic W_2BC phase was published starting in 2018. It was shown that sputter deposited W-B-C coatings of various compositions provide high hardness, and high elastic modulus [91–94]. The presence of the orthorhombic W_2BC phase was not reported in any study. The coatings exhibited several different structures, including fully amorphous structure [94], nanocrystalline structure composed of binary phases [93] or short-range ordering [91, 92].

Single report of the orthorhombic W_2BC phase was published by Wicher et al. in 2020 [95]. The finding was presented by fast Fourier transformation of the HRTEM image, which enabled determining the spacing between atomic planes. Four reflections can be matched with the nominal spacing of the W_2BC unit cell on the FFT. However, three of them are below the point resolution of the Tecnai G2 F20 S-twin transmission electron microscope used in the study, and the reflections overlap with other strong reflections of binary phases of tungsten, which makes the analysis highly unreliable.

Still, even the amorphous W-B-C coatings exhibited high hardness, and high elastic modulus, which was reported in [91, 92, 96] and in the author's publication 4.3. The hardness and modulus of the sputter deposited W-B-C coatings varied between $\sim$9-29 GPa and 130-440 GPa, respectively. Around the W_2BC composition, the coatings exhibited the hardness of $\sim$25 GPa and the modulus of $\sim$400 GPa with no residual stress. Several indicators also showed a higher fracture resistance compared to the state-of-the-art ceramic coatings [91, 92, 96] and together with the measurement of the damage parameter in 4.3 it hints high resilience of the W-B-C coatings.

Only a few studies concerning the Ta-B-C and Nb-B-C systems were published. The first study on the sputter deposited Ta-B-C coatings by Buršík et al. reported a hardness of 28 GPa and an effective elastic modulus of 442 GPa for an unspecified Ta-B-C coating. Based on H/E, H^3/E^2 values, and indentation-induced cracking, the study concluded the coating's increased fracture toughness and wear resistance. The Ta-B-C system was described in more detail in the author's publication 4.2. The study linked the structural and mechanical parameters to the industrially deposited Ta-B-C coatings composition. Only tantalum binary phases were detected by x-ray and electron diffraction and the coatings exhibited high hardness (up to 30 GPa) and modulus (up to 450 GPa). Even utilizing HiPIMS did not result in synthesis of Ta_2BC phase [98].

The sputter deposited Nb-B-C coatings were studied by combinatorial approach in a wide composition range [99]. Hardness and modulus varied between 8-23 GPa and 130-310 GPa, respectively. The formation of Nb, NbC, NbB_2 and Nb_2C phases was observed depending on the composition and energy available on the substrate [99].

2.4 Author's research of Me-B-C coatings

The author's doctoral research started in September 2018 and was focused on two Me-B-C coating systems, namely the system with tungsten (W-B-C) and tantalum (Ta-B-C). The properties of both systems were studied and described in the author's publications 4.2 and 4.3. Up to this day, these are the only studies that focused on the industrial deposition of W-B-C or Ta-B-C coatings. However, they also provided a thorough investigation of the coatings' properties to the scientific community.

Benefiting from the industrial cooperation, it was possible to study the properties of the coating and to provide an insight into industrial deposition process simultaneously. The publications 4.2 and 4.3 shared a similar approach to the research; they linked the composition of the coatings to the structural and mechanical properties.

The coating depositions were carried on the industrial batch-coater described in section 1.5. The research was conducted with the goal of possible deployment of the coating in the production manufacture of SHM, s.r.o. It implied developing a deposition process that included a complete description of the substrate preparation, pre-deposition cleaning, and deposition process parameters. Even though the development of the deposition process was not described in the publications, it was equally important as the material research itself and it included several aspects.

The choice of substrate was important. Since the coatings were tasked to serve as protective coatings on tools, the steel substrates were a reasonable choice. Due to the size of the sputtering source, the substrate is coated along 300 mm vertical and is under constant movement during deposition. The substrate needed to be firmly mounted vertically in the chamber, provide an almost seamless surface to be coated and optimized for the subsequent analyses. It resulted in custom substrates made from stainless ferromagnetic cold-rolled steel (AISI 304) with dimensions $40 \times 20 \times 3$ mm. The substrate holder was designed to mount seven substrate pieces in a single column to cover most of the deposition area. The steel substrates were utilized for most analyses. Custom holder was also designed for long silicon strips cut from Si(100) wafers, which were used for the analysis of stress, imaging, and to study the influence of the substrate on the deposited coating.

Even though the deposition process was not derived from scratch and was based on the manufacturer's vast experience, it underwent many changes to be suitable for the Me-

Coating analysis	Technique(s)	AISI 304S	Si(100)
Surface imaging	SEM	cross-verified	
Cross-sectional imaging	SEM, TEM, STEM		✓
Morphology	confocal microscopy	✓	
Composition	EDS	cross-verified	
Structure	XRD, SAED, TEM	cross-verified	
Mechanical properties	instrumental indentation	✓	
Residual stress	3D profilometry		✓

Table 2.5: Coating analysis according to substrate type.

B-C coatings. The first step was substrate preparation. The substrates were prepared for deposition by ultrasonic cleaning in degreasing agents and loaded into the chamber. The chamber and substrates were heated and evacuated to pressure $< 1 \cdot 10^{-3}$ Pa to outgas any volatile contaminants from the substrate.

Ion cleaning The ultrasonic cleaning and outgassing cannot remove all residues and contaminants, and the substrate is usually cleaned in the coater just before deposition. The accelerated ions are often used to etch the substrate and thus obtain a clean surface of the substrate. Initially, the metal ion etching was utilized for the deposition process of Me-B-C coatings, see figure 2.9a. Remote arc source generated titanium ions that were accelerated at -1000 V towards the substrates, which sputtered any contaminates on the substrate surface.

The metal ion etching was effective and ensured good adhesion of the coatings on steel and silicon substrates. However, it introduced seeds and surface irregularities, which resulted in nodular defects in the coatings. Consequently, such cleaning was concluded unsuitable because the defects in the coating acted as the weak points, where was a high probability of crack initiation [100]. It would lower the fracture resistance and, hence, conflicted with the primary purpose of the Me-B-C materials.

Other types of cleaning were thus searched for. The final version of the deposition process utilized cleaning by Ar ions using the LGD® (Lateral Glow Discharge) technology (figure 2.9b). The LGD® generated Ar ions by electron flow diverted from shuttered arc ionization source mounted in the coater [101]. The substrates were cleaned by an intense

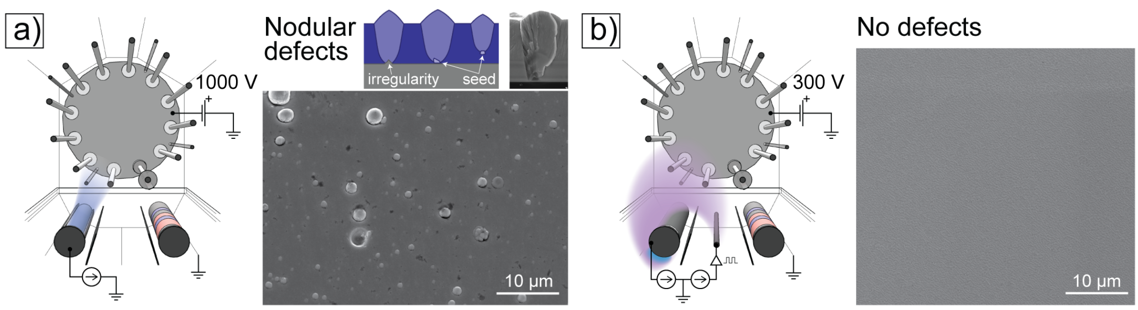

Figure 2.9: Schematic of a) metal ion etching and b) LGD® (Lateral Glow Discharge) cleaning methods. The SEM images show resulting coating surface when utilizing given method. Illustration of defects adapted from [100].

bombardment of Ar ions accelerated by $-300\,\mathrm{V}$ applied to the substrates. To put it in perspective, the etching speed of TiN coating and AISI 304S steel were $\sim$3 nm/min and $\sim$6 nm/min, respectively. The method provided a uniform surface without the seeds and defects on the substrate's surface and maintained very good adhesion of the coating.

Process parameters The deposition process parameters were predominantly based on the technical constraints of the batch coater and simultaneously had to fulfill demands given by the coating manufacturer. These applied to base pressure ($< 8 \cdot 10^{-3}$ Pa), input power (≥ 10 kW, include ramp-up), cathode voltage (< 800 V) and substrate temperature (< 450°C). A few technical limits were overcome by adapting the system and laboratory for this research. For example, the maximal deposition temperature could be increased by 100°C by adapting the central cooling loop and the batch-coater system.

The goal was to seek the parameter values that would enable obtaining the maximal available energy on the substrate to increase the adatom mobility and potentially favor the crystallization of the Ta_2BC or W_2BC phase. Substrates were, therefore, heated to 550°C and biased at -100 V. The argon pressure was 0.44 Pa, which was the low limit of a stable running process at the required 10 kW to increase the mean free path of sputtered particles. The description of the deposition process illustrates figure 2.10.

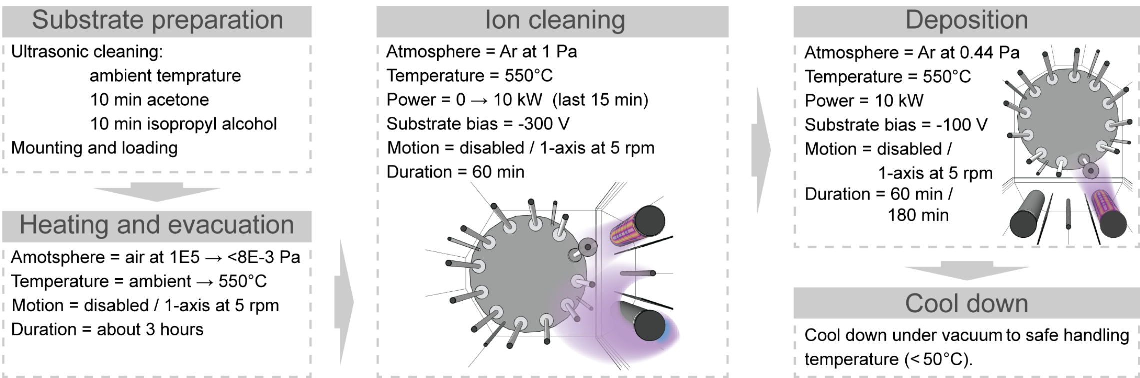

Figure 2.10: Diagram of the substrate preparation, ion cleaning and deposition process parameters utilized to industrially deposit W-B-C and Ta-B-C coatings.

Deposition regimes The preceding author's publication 4.1 reported and described inherent multilayering caused by the motion of the substrate. The motion caused modulation of the coating composition, and depending on its type, the resulting multilayering was different. The coatings deposited with 2-axis rotation exhibited more complex layering than the coatings with 1-axis rotation.

Following these findings, the samples for publication 4.2 and 4.3 were prepared in two deposition regimes. The first was a stationary regime with no substrate motion. The coatings were expected to be the mono-block without any modulation of the coating composition in the growth direction. The second regime employed the 1-axis rotation of the substrate, and coatings would thus exhibit a fine multilayered structure. Therefore, a comparison could be made between the mono-block and the multilayered coatings, which are expected to form inherently during an industrial deposition process.

The fine multilayered structure was confirmed by TEM for both W-B-C and Ta-B-C coating systems. Suffice it to say the influence of substrate rotation was not negligible and could be detected on the coating properties. However, their changes were not major for most compositions of W-B-C or Ta-B-C coatings, and general trends of structural and mechanical properties were maintained regardless of the deposition regime.

Ta-B-C and W-B-C coating properties Utilizing the combinatorial approach described in section 1.5 allowed studying coatings with various chemical compositions while keeping the process parameters constant. The segmented targets were designed to attain a composition gradient with varying content of metal or varying boron to carbon ratio in the coating. Two target setups for deposition of W-B-C and Ta-B-C were identical, and their chemical composition thus shared similar evolution. The metal content in the coatings was, however, different. The Ta-B-C coatings exhibited lower content of metallic constituent than the corresponding W-B-C coating, which was the manifestation of the lower sputtering yield of tantalum.

The microstructure of Ta-B-C and W-B-C coatings exhibited substantial differences. The W-B-C coatings exhibited low to no presence of any crystalline phase. With high carbon and high tungsten content, they showed the formation of nanocrystalline c-WC. For the coatings with high boron content, the x-ray (XRD) and electron diffraction indicated the start of crystallization of the tungsten boride and diboride phases. However, these were not possible to unambiguously identify because the coatings exhibited only short-range ordering of atoms. Most of the W-B-C coatings were amorphous.

On the other hand, the Ta-B-C coatings exhibited polycrystalline structure for a wide range of compositions. They were composed of binary tantalum phases of boron or carbon – TaB, TaB_2, and TaC. High tantalum content favored the formation of tantalum carbide, and with a small content of tantalum, the coatings were amorphous or nanocrystalline.

Revisiting the findings from the DFT calculations, the Ta_2BC phase should have benefited from more negative formation enthalpy compared to the W_2BC and Mo_2BC phases and thus favor its crystallization. However, this applied to the tantalum binary phases as well.

Table 2.6 shows calculated formation enthalpies of the ternary Me_2BC phases and binary phases of tungsten and tantalum, which were indicated in the coatings. Clearly, the formation enthalpies of tantalum phases were more negative than the tungsten phases and, thus, more likely to obtain. Note that the calculated formation enthalpies in table 2.6 are somewhat indicative because they represent structures at 0 K. In the case of the c-WC, the formation enthalpy is even positive, indicating an unstable phase, which contrasts

W-B-C

Phase	Space group	H_F (eV/atom)
WB	$I4_1$/amd (141)	−0.368
WB_2	P6/mmm (191)	−0.075
c-WC	Fm$\bar{3}$m (225)	+0.325
W_2BC	Cmcm (63)	−0.161

Ta-B-C

Phase	Space group	H_F (eV/atom)
TaB	Cmcm (63)	−0.813
TaB_2	P6/mmm (191)	−0.649
TaC	Fm$\bar{3}$m (225)	−0.576
Ta_2BC	Cmcm (63)	−0.678

Table 2.6: Formation enthalpies at 0 K of tungsten and tantalum phases. Data taken from [35] for ternary phases and [102] for binary phases.

with the experimental observation. The crystalline structures may be stabilized at higher temperatures or by vacancies introduced into the structure and therefore be experimentally observed, which is likely the case of c-WC. On the other hand, the ternary phases should be stable according to their formation enthalpies, and the enthalpy of Ta_2BC phase is even lower than some observed phases within the Ta-B-C system. However, the x-ray and electron diffraction did not provide any evidence of the ternary phases formed in the coating for both the W-B-C and Ta-B-C systems.

The formation of the binary phases introduced intrinsic compressive stress to the Ta-B-C coatings. At tantalum content > 40 at.%, the residual compressive stress was as high as 9 GPa. Fortunately, the adhesion on the steel and silicon substrate was sufficient, and the adhesion failure was never encountered. The combination of the high residual stress and strong adhesion to the substrate caused visible bending of the silicon samples and, in some cases, destruction of the sample due to excessive mechanical stress applied to the substrate. The W-B-C coatings generally exhibited lower compressive stress. The amorphous W-B-C coatings were stress-free.

Both systems were capable of providing high hardness with a high elastic modulus at specific compositions and thus were considered hard protective coatings. The polycrystalline Ta-B-C coatings reached higher hardness (up to 30 GPa) and modulus (up to 450 GPa) values than the W-B-C coatings. But the fracture resistance of the tantalum-based coatings was on par with state-of-the-art coatings.

The W-B-C coatings provided reasonably high hardness ($\sim$25 GPa) and elastic modulus ($\sim$400 GPa) even with an amorphous structure. The absence of intrinsic stress enabled depositing coatings with thickness exceeding 40 μm, which allowed measuring their damage parameter. The damage resistance of W-B-C coatings was substantially better than that of the TiN, and it outperformed the AlCrN. The observed deformation on residual imprints shared similarities with the deformation of metals, implying increased fracture and damage resistance of the amorphous W-B-C coatings.

The publications 4.2 and 4.3 showed that ternary Ta-B-C and W-B-C coating systems provide a range of parameters, which could be tuned with their chemical composition. Since these coatings could be prepared by a simple non-reactive process and the deposition from the segmented target was feasible, high flexibility and easy industrial deployment were thus achieved.

The objective of achieving high toughness together with moderate ductility was not accomplished for the Ta-B-C system. In the retrospective, the Ta-B-C system could have been researched more thoroughly as the composition Ta_2BC was not approached, and the samples exhibited tantalum content up to 45 at. %. However, considering the observed evolution, the formation of the Ta_2BC phase was not probable because the tantalum carbide was formed in the coating close to the Ta_2BC composition. Moreover, the exceptionally high residual stress did not favor any intended application and would have to be addressed prior to the deployment in the industrial production. With the high economic cost of tantalum metal for target segments, the Ta-B-C coating system was not considered for continuing research.

On the other hand, the properties of the W-B-C coatings, specifically those with composition around W_2BC stoichiometry, are very close to the promising features of the

W_2BC phase, even though they are amorphous. Because the properties of the amorphous coatings are not strongly dependent on the deposition regime and coating composition, the deposition process can be robust.

2.4.1 Industrial testing of the W-B-C coatings

The deposition of the W-B-C and Ta-B-C coating using the segmented target is a verified technology that enables the preparation of coatings with a broad range of properties. The SHM, s.r.o. utilized the technology for commercial purpose. After consultations, the coating from the W-B-C system was chosen for further testing directly in the SHM, s.r.o. The composition of W_2BC was selected due to the desirable properties and the fact that a small variation in the coating composition will not change these properties significantly, which makes the deposition process robust.

The W_2BC coating is amorphous with hardness and effective elastic modulus ~25 GPa and ~400 GPa, respectively. It exhibits 0 GPa of residual stress and higher damage resistance than the AlCrN and TiN coatings.

Several samples were prepared on the steel substrates in the SHM, s.r.o. to verify the properties of the W_2BC coating and compare them with the samples from Masaryk University. The depositions were carried out on the identical sputtering system equipped with the same sputter source. The setup of the segmented target was adapted for the coating production because it had to provide close-to homogeneous composition of the coating along the vertical axis of the chamber.

The design was based on the simulation of the coating composition, which is described in the next chapter. The target setup and coating composition are shown in figure 2.11. The coating composition is not ideally homogeneous because the available sizes of target segments did not allow for better homogeneity at that time. Further optimization of the homogeneity can be performed with precisely crafted segments to defined sizes, which can be obtained with help of the simulation tool.

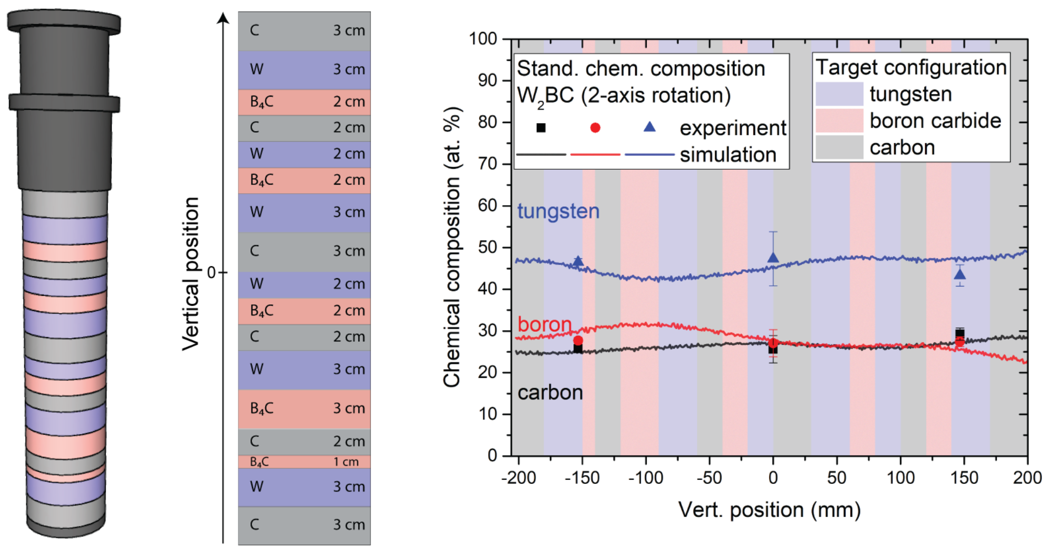

Figure 2.11: Target setup for deposition of W_2BC and resulting composition of the coating.

The coating production employs the random 2-axis rotation, which ensures the coating uniformity on tools with more complex geometries than the flat samples. Therefore, the coating exhibits a multilayered structure. However, the properties are not significantly different when comparing the multilayered and mono-block W_2BC coatings. Figure 2.12 shows the comparison of mechanical properties of coatings prepared at the university and the SHM, s.r.o. The coatings' properties matched, which verified the process's repeatability and robustness.

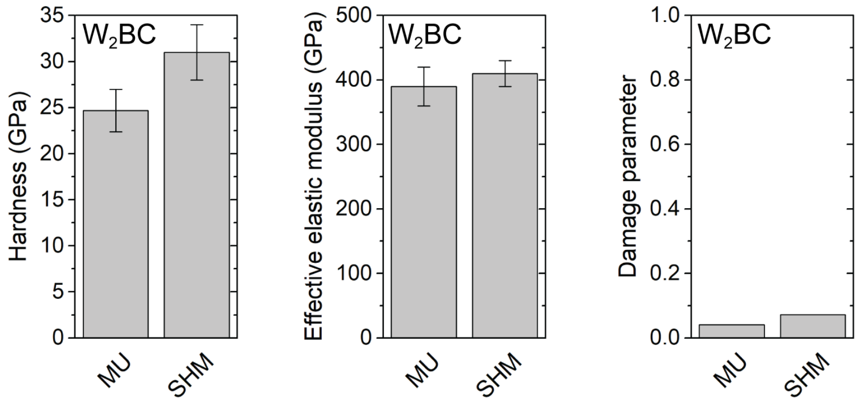

Figure 2.12: Comparison of mechanical properties of the W_2BC coatings prepared at Masaryk University (MU) and SHM, s.r.o. (SHM).

Dual coating system Commercial top-shelf coatings are very often systems of several materials, where each material possesses different properties that complement each other and serve different purposes. They are usually composed of an adhesion layer, core coating, and top coating.

In this case, a similar approach was investigated. The W_2BC coating was paired with nitride coating, which exhibited higher hardness but lower damage resistance. The idea was to mitigate brittle fracture and utilize the W_2BC to stop crack initiation and propagation through the coating system because it can withstand more damage without cracking. The SHM, s.r.o. utilized ALWIN® nanocomposite coating, which is based on the AlCrN material and commercially offered. It is a coating with high oxidation resistance and resistance to sticking of the machined material applicable for stamping, pressing, and drilling or machining metals.

The W_2BC adheres very well to the substrates. Therefore the adhesion layer is unnecessary, and the coating can be applied directly on the ion-cleaned substrates. The testing showed that the W_2BC and ALWIN® could be applied to each other, and their interface did not exhibit any delamination or defects. Therefore, it was verified that the W_2BC and ALWIN® coatings could be combined in the dual coating system.

Figure 2.13 presents two examples of dual coating systems of W_2BC-ALWIN® coatings. The first example (figure 2.13a) is 5 µm ALWIN® coating deposited on the top of the 3 µm W_2BC coating, which serves as the core coating without any adhesion layer. The second example (figure 2.13b), is the W_2BC-ALWIN multilayered system with ALWIN® as the top coating. The figure shows a cross-sectional SEM image of the coating system prepared on silicon and optical microscope images of the ball crater milled in coating prepared on the steel substrate.

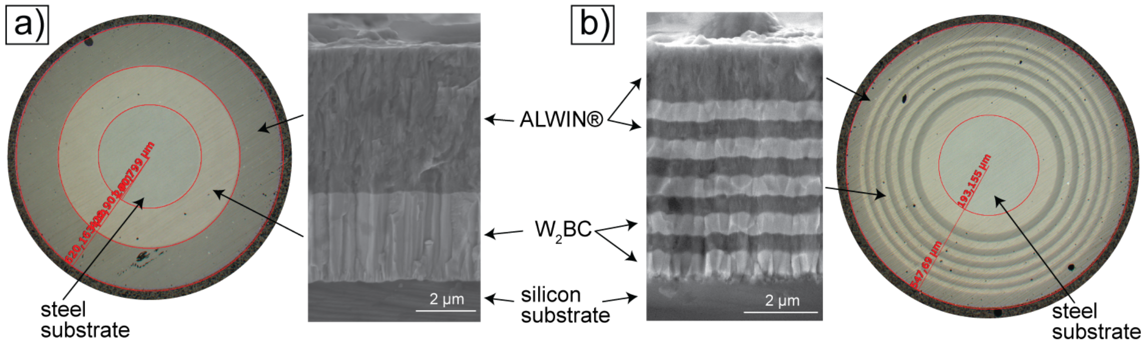

Figure 2.13: Examples of dual coatings prepared during industrial testing a) ALWIN® on the top of W_2BC coating b) multilayered W_2BC + ALWIN®.

Pre-production testing The main advantage of the W_2BC coating lies in its damage resistance. It can be plastically deformed to a great extent by mechanical load without inducing severe damage by cracking or chipping. Therefore, the main area of potential application is metal forming, where the integrity of the tool surface is crucial. The intended use of the coating includes stamping, shearing, bending, etc.

Pre-production testing was performed by SHM, s.r.o. with several customers willing to participate in the testing and thus deploy tools with this new type of coating that could exhibit high performance in their production. Examples of testing tools are shown in figure 2.14. The images capture tools mounted on the substrate holders that perform 2-axis rotation during deposition process.

The goal of SHM, s.r.o. was to asses the coating performance and gather customer feedback. If the customer utilized another type of protective coating on the tested tool, the performance of the new coating was compared to the previously used one. Where the direct comparison could not be performed, customer expectations were the main indicator.

Table 2.7 summarizes the pre-production testing at four customers. The deployed coating at customers always combined the W_2BC and ALWIN® in the dual coating system. The tested coating system was applied to the forming mandrels at Industrial Machining

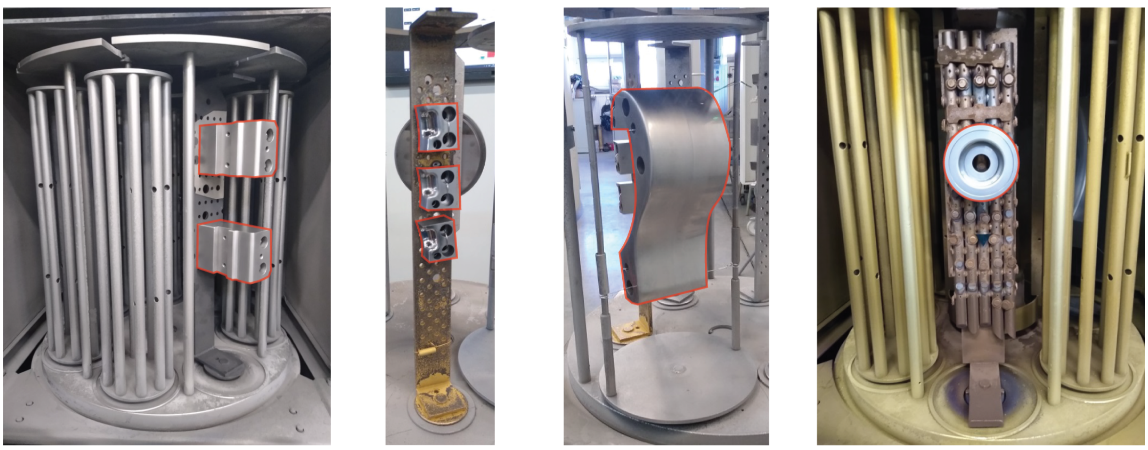

Figure 2.14: Examples of testing tools mounted on the substrate holders.

s.r.o., it utilized the W_2BC as the top coating. The testing revealed one particular issue with this coating system. The performance was limited because the W_2BC adhered to the work material. Upon sticking, part of the coating was torn from the tool. The tool's surface was comprised after a few cycles, and the mandrel could not be further used without renewing the tool's surface. Therefore, the W_2BC is more suitable as a core coating than a top coating, so contact with the work material is prevented.

The coating system with the ALWIN® as a top coating showed better test results. The Magna Automotive s.r.o. utilized the coating on tools used for forming vehicle frames and control arms of the suspension system. The coated calibration punches for vehicle control arms recorded a production increase. The production increase with W_2BC-ALWIN® coated tool was up to 30% (measured by the count of processed parts with a single coated tool). The performance of the coated bending dies inserts for car frames fulfilled the customer's expectations, and further testing was requested.

High satisfaction was reported by METECH s.r.o., which utilized the W_2BC-ALWIN® coating for punch shearing dies. The coated tools did not show any wear after 15k cycles and its lifespan was higher than 74k cycles, which exceeded the customer expectations. The W_2BC-ALWIN® was also tested for deep drawing dies of sheet metal at LUR - KOVO Zacpálek s.r.o., which reported high tool lifespan.

Even though searching for a suitable application is beyond the scope of this doctoral research, several test cases showed that the new coating for particular applications outperformed previously used protective coatings or provided satisfactory performance. The SHM, s.r.o. was the first manufacturer to deploy this new type of coatings. They possess the technology for optimizing the coating properties further and potentially creating an industry-leading product.

Customer (Coating)	Parts	Test results
Industrial Machining s.r.o. (ALWIN® + W_2BC)	forming mandrels	immediate coating adherence to work metal
Magna Automotive CZ s.r.o. (W_2BC + ALWIN®)	calibration punch	616k cycles (30% increase than TiAlCN coating)
	bending dies inserts	fulfilled expectations, more coated parts requested
	bending dies inserts	testing requested
METECH s.r.o. (W_2BC + ALWIN®)	punch shearing dies	64k cycles, part approved for next 10k cycles
LUR - KOVO Zacpálek s.r.o. (W_2BC + ALWIN®)	deep drawing dies	fulfilled expectations

Table 2.7: Summary of application tests at customers.

Chapter 3

Simulation of the sputtering process

Advances in computer science and numerical methods opened the possibilities to implement the laws of physics in the computer code and develop meaningful physical models. It enabled scientists to derive predictions and observe relations prior to conducting the experimental work and even provide insight beyond the physical limits of real-life experiments. Modern computers provide sufficient power and make modeling available to the broad scientific community because a personal computer is often sufficiently powerful to finish various simulations in a reasonable time.

The best case scenario is when the modeling and experimental work is bound together in a single effort because the simulations decrease the time and cost of the experimental research for example by ruling out unsuitable approaches or pointing out key parameters and relationships. The modeling may also reveal and explain phenomena that play a crucial role and are not directly observable by the experiments. On the other hand, the experimental work provides inputs for the models and increases their accuracy by calibrating them with the experimental data, making the model more reliable and usable.

The modeling efforts are also focused on the deposition of coatings. Modern deposition techniques are based on plasma-matter interactions, enabling the plasma modeling to derive parameters relevant to the deposition process and relations between the process and plasma parameters. The global models can describe the properties of the process without considering the geometry of a particular problem, which significantly decreases the computational cost [103]. Models with full three-dimensional spatial resolution provide higher accuracy and benefit from direct comparison to experimental data, but such models are substantially more demanding.

In the particular case of magnetron sputtering, a magnetized plasma must be assumed, which complicates the models quite a bit. However, the plasma itself may not even be considered to develop a meaningful model for the deposition process. The sputter deposition process can be divided into three parts for the purpose of modeling: i) sputtering of the target; ii) transport of the particles; iii) growth of the coating. The focus is given to the first two parts in the following text because these determine the composition of the coatings. By assuming the sticking coefficient of 1, the coating growth is effortlessly solved for the purpose of simulating the coating composition.

Modeling the growth of coating and its properties is possible but highly challenging as it requires complex atomistic and quantum simulations often supported by molecular dynamics. An example was already shown in the section 2.1, where the prediction of mechanical properties of Me_2BC crystalline phases was described. Optical properties or electronic structure may be derived in similar manner [104]. Apart from the ab-initio approach, the coating parameters may also be linked by empirical relations or machine learning to a coating composition and process parameters [105].

3.1 Target sputtering

Even though the sputtering is often based on electric discharge that generates plasma, in essence, it is an ion bombardment of a target, what causes a collision cascade that leads to releasing target atoms to the vapor phase. The probability of the release is described by the sputtering yield, which depends on the target material, ion species, their energy, and the angle under which they impinge on the target. In the case of magnetron sputtering, the ion energy is determined by the cathode voltage, and the angle can be assumed normal because the ions accelerate in a thin cathode sheet.

However, the sputtering yield is strongly connected to the target material, mainly to its composition, surface binding energy, and density. It determines the sputtering efficiency and consequently affects the composition of the coating. It is an essential parameter to input in the simulation of the deposition process.

Although the experimental methods for measuring the sputtering yield do exist, the variety of materials utilized for sputtering is not likely to be covered soon. However, the ion-matter interaction, including the collision cascade, can be calculated. The collision cascade may be understood as a transport of the particles through matter in a solid state and thus be approximated with a set of binary collisions – binary collision approximation (BCA).

Well-known freeware BCA codes, which are based on the Monte Carlo method, are SRIM/TRIM [106], TRYDIN [107], and SDTrimSP [108]. They differ in capabilities and user interface, but all are concerned with features of the transport of ions in the matter and thus share the same physics. These three codes can calculate the collision cascade and simulate the sputtering of the target material. They assume a randomized target at 0 K, i.e. amorphous target composed of static target atoms. The SRIM/TRIM provides an easy-to-use graphical user interface, making it widely used. Whereas the TRYDIN and SDTrimSP are, in default, controlled with a command-based interface but offer more features that focus on sputtering.

The TRYDIN and SDTrimSP are capable of dynamic calculations, which consider the target's chemical changes that may occur during sputtering. The ion implantation is present to some extent because the collisions stop the ions within the target, changing its composition. Furthermore, in the case of the compound targets, the mismatch of sputtering yields of individual elements leads to the formation of a near-surface layer with a different composition than the target bulk. The dynamic simulations periodically assess the composition changes and update the depth profile of the target accordingly, pushing the simulation closer to the reality.

The SDTrimSP code was developed by Mutzke et al., and it implements additional modules that increase the accuracy and usability (thermal diffusion, models for target outgassing, several surface binding energy models, and more). It also includes a com-

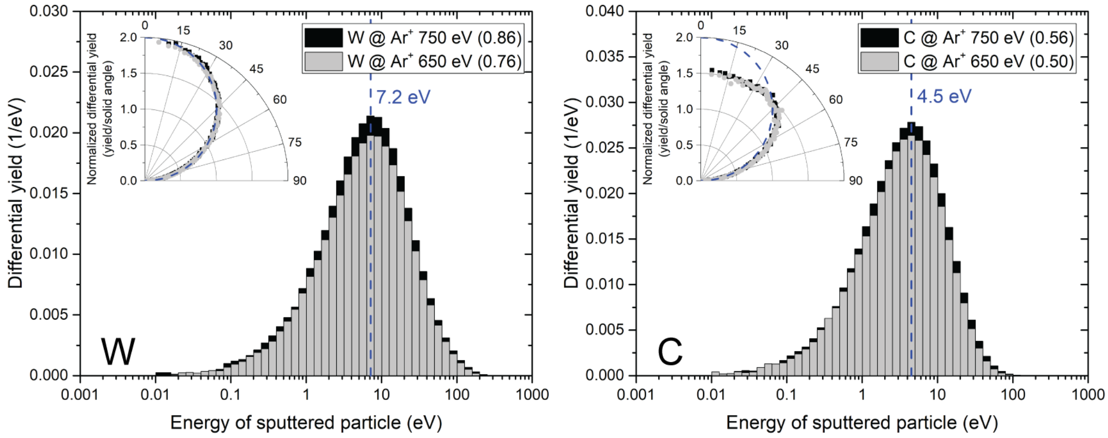

Figure 3.1: Differential sputtering yields according to the energy and ejection angle for a) tungsten and b) carbon.

prehensive internal database of single-element materials and some popular compound materials. The SDTrimSP calculates the sputtering yield and provides energy and angular distribution of the sputtered particles. It derives more accurate results for sputtering of low *Z* elements at energies relevant to the magnetron sputtering [109].

The distributions are usually converted to differential sputtering yields, which serve as the initial condition for particle transport simulation. Figure 3.1 depicts examples of the simulated differential sputtering yields according to the energy and ejection angle for tungsten and carbon. The results are derived from the SDTrimSP simulation for argon bombardment of the carbon and tungsten targets with ion energies 650 eV and 750 eV. The sputtering yields for tungsten and ion energies of 650 eV and 750 eV are 0.78 and 0.86, respectively; for carbon, the calculated yields are 0.50 and 0.56.

The energy distribution correlates with Thomson distribution [110], and it increases in full energy scale for the case of 750 eV for both materials. However, the tungsten and carbon are sputtered differently. The tungsten atoms are ejected with higher energy and exhibit close to ideal cosine distribution. In contrast, the carbon exhibit highly under-cosine distribution, indicating it is sputtered to wider angles than the tungsten. Such differences in sputtering yields influence the deposition process, and gaining this data is highly beneficial for experiments and almost essential for the simulation of deposition process.

The SDTrimSP and its alternatives allow for obtaining valid data for the sputtering, but the limits must be understood. Without modifications, the target is assumed amorphous; it cannot thus comprehend the effects of crystal orientation or changes in the target's structure like recrystallization or bond formation in compounds. The ideally flat target in simulations cannot account for the roughness effect, which also impacts sputtering yields [111]. The simulated sputtering yields are always approximate and must be understood in accordance with this fact.

In case of magnetron sputtering one more aspect needs to be considered. The particles are not sputtered evenly from the target. The magnetic field determines the intensity of sputtering and therefore the number of sputtered particles. The field is not designed homogeneous, which consequently creates the racetrack. The geometry of the racetrack must be thus implemented in simulations. It can be estimated from the visible erosion trench only in the case of stationary targets, but it can also be determined from the magnetic field of the sputter source.

The direct measurement of the tangent component of the field strength requires sufficient spatial resolution to derive the racetrack geometry, which is time-consuming. There are also computational methods that can determine the distribution of the magnetic field based on the placement of permanent magnets or coils to derive the geometry of the racetrack [112, 113].

3.2 Particle transport

The transport of the particles takes place between the target and the substrates. The sputtered particles are ejected from the target and propagate through the chamber onto a substrate, where condensate and create the coating. The working gas is a medium through which the sputtered particles must propagate to reach a substrate.

During transport, the sputtered particles collide with the atoms of the working gas and are scattered on them. The deposition pressure and temperature determine the density of the working gas atoms and, therefore, the mean free path of the transporting particles. Since the pressure of the working gas is typically between 0.01-5 Pa, the binary collision approximation can be utilized to simulate the gas phase transport.

The transport of a simulated particle starts on the target surface with initial conditions given by the energy and the ejection vector gained from the differential sputtering yield. The particle free path is derived based on the mean free path and random number. After traveling the distance of the free path, it undergoes collision with a gas atom, then the scattering angle and new velocity are calculated according to the collision description. It is repeated until the particle reaches the substrate or any other surface.

The examples of gas phase transport simulation are shown in figure 3.2. The particles are transported from flat circular target (⌀120 mm) through a simulation cell filled with argon gas at pressure of 1 Pa and temperature 550°C. The particles are of different masses

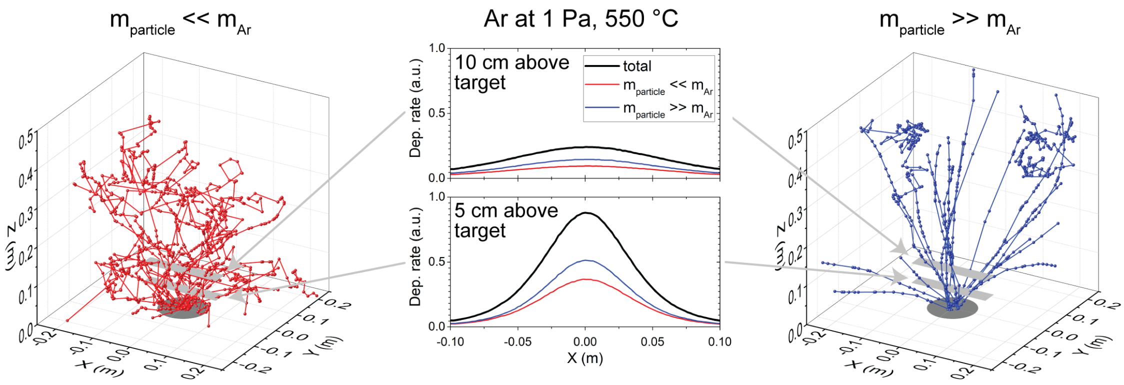

Figure 3.2: Simulation of sputtered particles transport in argon atmosphere at 1 Pa and 550°C for particles lighter (left) and heavier (right) than argon. Graphs show deposition rate at 5 cm and 10 cm above the target. Simulated using SiMTra [114].

to show different transport characteristics and the influence on the deposition rate.

The lightweight particles exhibit higher scattering on the gas atoms, meanwhile the heavy particles are transported along more straight trajectories. As a result lightweight particles exhibit higher loss on the walls and thus smaller deposition rate on the substrate. The deposition profiles also show how the target-substrate distance affects the deposition rate. The simulated substrates were 20×200 mm flat surface placed 5 cm and 10 cm above the target surface. At longer distance, the deposition rate is significantly lower, but more homogeneously distributed.

A complete toolkit for the particle transport simulation is the SiMTra code [114], developed within the prof. Depla's DRAFT research group at the University of Ghent in Belgium [114]. The software focuses explicitly on magnetron sputtering and enables designing custom 3D geometries of the vacuum chamber, sputter source, and substrate.

The material parameters, type of working gas, its pressure and temperature serve as inputs. Fundamentally, the working gas atoms are assumed static, and the collective gas motion effects are thus not considered in the simulation, therefore, the gas rarefaction is omitted. The racetrack is mapped on the sputter source by a probability map, and initial conditions are inputted directly from the target sputtering model in SRIM/TRIM format or by setting the theoretical distributions.

The SiMTra outputs the deposition profiles on substrates and is also capable of tracing the trajectory of the simulated particles. The code allows simulating the transport of single species from a single sputter source at the same time. However, it is also possible to derive the composition of multi-element coatings by combining the outputs of a set of individual simulations.

3.3 Comments on author's relevant publications

The segmented cylindrical target utilized for the W-B-C and Ta-B-C coating research provided high flexibility and enabled the combinatorial approach. The placement and size of segments determined the resulting composition of the coating. Designing a target setup, that would exhibit compositional gradient, could be performed based on a rough estimate, e.g., place first material on one side, second material on the opposite, and interlace them with third material.

However, designing a segmented target to obtain the desired composition is difficult. It is even more challenging in the case of targets for coating manufacture, which has to provide the nominal composition, that is constant within the whole coated region. The design of segmented target is almost impossible to base reliably on experience because the sputtering yield and shape of the racetrack has considerable affect on the composition.

Publication 4.4 presented an approach for simulating the composition and relative thickness of the W-B-C coatings deposited from the segmented target. The approach was based on freeware SDTrimSP and SiMTra. The SDTrimSP derived the sputtering yields of tungsten, carbon, and boron carbide and the angular and energy distributions of sputtered particles. The SiMTra simulated the transport of particles from the target to the substrates and implemented the sputtering system's geometry and racetrack geometry. The process parameters of the simulations were identical to the experiment. The approach followed the block diagram shown in figure 3.3.

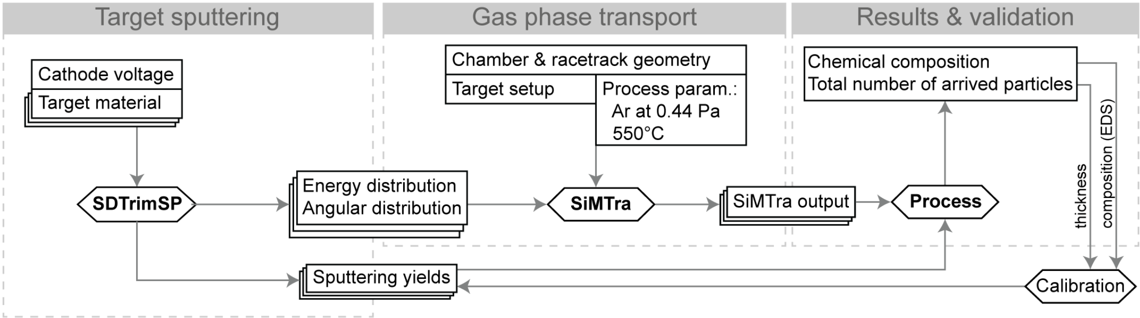

Figure 3.3: Procedural diagram of the developed simulation approach.

To determine the racetrack geometry, a pole sensor foil was used to visualize the magnetic field on the target. The determined region, where the magnetic field is parallel to the target surface, was correlated to the racetrack, see figure 3.4. The image of the foil was digitized and converted to the probability map usable within the SiMTra as the racetrack. The probability map and more details are described in publication 4.4.

Since the SiMTra does not support the multi-element targets, the simulations had to be performed individually for each element of every target material. For the target composed of tungsten, carbon, and boron carbide materials, a total of 4 simulations were needed – B atoms from boron carbide segments, C atoms from boron carbide segments, C atoms from carbon segments, and W from tungsten segments.

By combining the SiMTra outputs and sputtering yields obtained by SDTrimSP, it was possible to simulate the composition and relative thickness of the W-B-C coatings as a function of position in the vacuum chamber. Stationary and 1-axis rotation regimes were simulated in the SiMTra. Rotation was implemented by discretization of the motion and integration of the composition.

The approach was developed with experimental results from two target setups for deposition of W-B-C coating (setup 1 and 2 from publication 4.3). Initially, the modeled composition did not achieve high accuracy, the trends were similar, but the boron content was underestimated. By looking back at the experimental apparatus it was found that boron carbide segments exhibited higher erosion than carbon segments, even though, the sputtering yield calculated by SDTrimSP was lower.

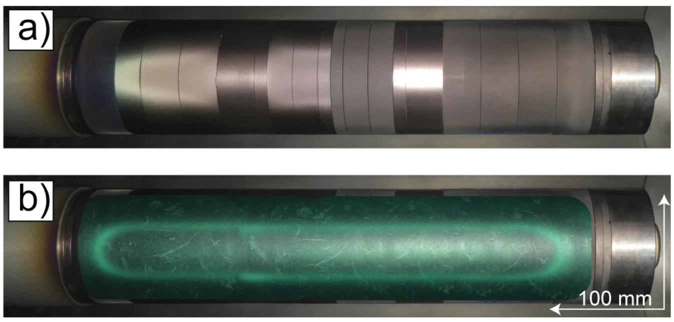

Figure 3.4: Image of a) segmented target mounted to the sputter source with b) pole sensor foil placed over the target. Brighter areas on foil correspond to the parallel magnetic field.

Increasing the sputtering yield of boron carbide by a fixed factor significantly improved the accuracy of the simulation. The modeled composition and relative thickness then matched the experimental data within a few %. Therefore the model was calibrated. The calibrated model even showed a minor decrease in tungsten content in the coatings when switching from the stationary to 1-axis rotation deposition regime, as it was observed in the experiment.

Using the calibrated model, it was possible to design the target setup 3, which fixed the tungsten composition at ∼50 at.%. Many targets were simulated and ruled out prior to conducting the experiments with setup 3. In addition, it enabled to design homogeneous setup of the target for two different compositions of the W-B-C coatings, thus easing the industrial deployment.

Simulation undoubtedly provided practical benefits for experimental work and industrial use, but scientifically valuable findings were also derived. Tracing the trajectories of simulated particles revealed differences in the transport of tungsten atoms and boron/carbon atoms. That strengthened the hypothesis stated in the article 4.1 about the origin of the multilayered coatings. The simulation approach is not limited to the W-B-C coatings, and all it needs is to create the database of materials and their sputtering yields. It was successfully tested on the segmented Si-C, Ta-B-C and Ti-Zr targets. The simulation of Ti-Zr target sputtering is described below.

Two cases were studied: sputtering of Ti-Zr target in Ar atmosphere and sputtering in Ar + N_2 atmosphere. Figure 3.5 shows the ratio of titanium to zirconium content in the coatings prepared from the Ti-Zr segmented target. The simulated composition of coatings deposited in the Ar atmosphere matched very well, which presents the graph in figure 3.5b. In the case of sputter-deposited coatings in the Ar + N_2 atmosphere, the developed approach cannot derive the nitrogen content or assume chemical reactions. However, the sputter source was operated at a high flow of nitrogen gas, which fully poisoned the target. The titanium and zirconium segments thus could be assumed as the binary nitrides. The sputtering yields of these compounds are different when compared to metals. Consequently, it shifts the content of metals in the coating to a higher concentration of zirconium. The simulation predicted this shift, which shows figure 3.5c and thus the method can also support observations of reactive deposition process to some extent.

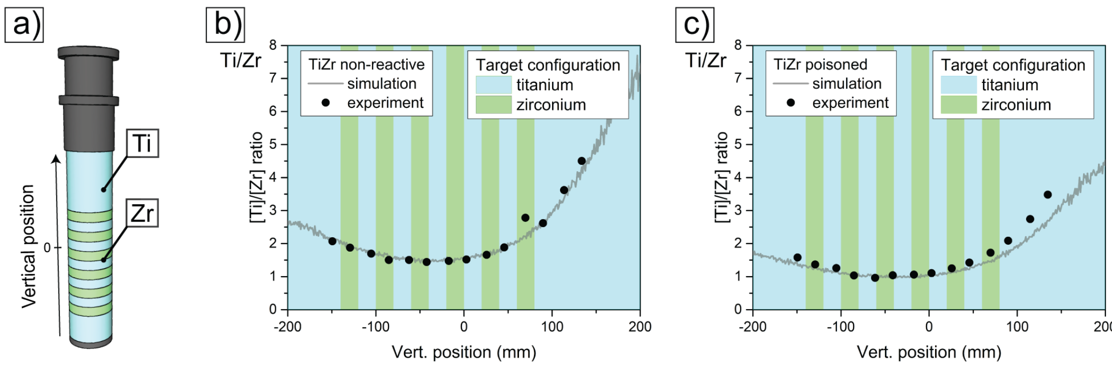

Figure 3.5: The case study of sputter deposited coatings from a) TiZr segmented target. Graphs shows the actual and simulated Ti/Zr ratio of sputter deposited coatings in b) Ar atmosphere and c) in Ar + N_2 atmosphere (poisoned target).

Benefiting from the knowledge and experience gained with SDTrimSP, the author contributed to other publications concerned with reactive HiPIMS and the hybrid PVD-PECVD process. During HiPIMS, a considerable amount of sputtered atoms are ionized and back-attracted to the target, thus contributing to sputtering – the so-called self-sputtering [115]. Moreover, due to the high ionization degree, one must often account for multiply charged ions as well [116]. The SDTrimSP calculated yields for sputtering of titanium target by working and reactive gas ions and self-sputtering yield and provided them as a function of cathode voltage. These calculations were utilized in the co-authored publications 4.5ii) and 4.5iii).

In the publication 4.5iii), a complex PVD-PECVD process was approximated using the SDTrimSP. It was, in essence, reactive sputtering of titanium target with argon as a working gas and acetylene as a reactive gas. The acetylene molecule impinging the titanium target was assumed fully dissociated and thus approximated by the two thermalized carbon atoms. The simulation calculated simultaneous sputtering by the argon ions and sticking of carbon atoms. The relative composition of the incident particles was determined from the adapted Berg model and derived as a function of reactive gas flow rate. Composition at the target surface was derived from the simulation, which showed an identical trend to the adapted Berg model and experimental results.

Chapter 4

Author's publications

The author contributed to seven full-length articles in total, four being the first authored and the other three co-authored. This chapter includes prints of the first-authored articles sorted in order of appearance in the dissertation, where they were commented on. They are devoted to the research activities during the author's doctoral studies of the Me-B-C coatings and were published in high-impact journals *Surface & Coatings Technology* (Q1) and *Coatings* (Q2). Three co-authored articles were published in *Plasma Sources Science and Technology* (Q1) and *Journal of Physics D: Applied Physics* (Q2).

The author's research was also presented publicly at international scientific venues multiple times: three oral presentations were given by the author, two additional contributions were presented in poster form, and three talks were co-authored. He is also the co-author of three other contributions on different topics. List of conference contributions is appended on page 120.

Contents

4.1 On the origin of multilayered structure of W-B-C coatings prepared by non-reactive magnetron sputtering from a single segmented target

DOI: 10.1016/j.surfcoat.2019.07.077

Published: August 2019

Journal: Surface & Coatings Technology

Impact factor in year of publication: 3.784

Authors: M. Kroker, Zs. Czigány, Z. Weiss, M. Fekete, P. Souček, K. Balázsi, V. Sochora, M. Jílek and P. Vašina

Author's contribution:
The author was responsible for the experimental work and the design of the deposition process. He carried out the depositions of the W-B-C coatings and discovered unexpected coatings' multilayered structure, which was the central topic of the publication.

The multilayering was assumed to originate from the substrate rotation. The author designed an experiment for video capturing the substrate motion. He described the substrate motion and chose three of its types to investigate for the purpose of this publication.

The W-B-C coatings were investigated by several analytical techniques. The author performed the scanning electron microscopy of coatings cross-section, including the specimen preparation and composition measurement by energy dispersive spectroscopy. He connected the multilayered structure with the substrate rotation by calculating the thickness increment per single rotation and comparing it to the thickness of the individual layers visible on the transmission electron microscope images.

Experiments with no substrate motion revealed that the composition of the coating is dependent on the position within the chamber. The author proposed and described the existence of the two regions within the chamber. The first region faced the sputtering direction, where the deposition rate is high, and tungsten-rich coatings are deposited; the second region averted from the sputtering direction, where tungsten-deficient coatings are deposited at a lower rate in comparison to the first region.

Visualization of data, together with the illustrative figures, and the sputtering system's 3D model, were created by the author, who took the lead in writing the original draft. He handled the publication and revision process of the submission with inputs of all co-authors.

4.2 Composition, structure and mechanical properties of industrially sputtered Ta-B-C coatings

DOI: 10.3390/coatings10090853

Published: August 2020

Journal: Coatings

Impact factor in year of publication: 2.881

Authors: M. Kroker, P. Souček, P. Matej, L. Zábranský, Zs. Czigány, K. Balázsi and P. Vašina

Author's contribution:
The author prepared the experimental methodology and concept of the research to investigate the industrially deposited Ta-B-C coatings. He designed the deposition process, which ensured the repeatability and sufficient adhesion of the coatings to the silicon and steel substrates. Segmented targets were assembled according to the author's design to obtain the composition of coatings with i) varying boron to carbon ratios and ii) varying tantalum content. The SHM, s.r.o. according to the author's specifications developed and manufactured suitable substrate holders and modified the system's control software.

The author conducted depositions of the Ta-B-C coatings in the stationary and 1-axis rotation regimes. He handled the sample curation and managed their transfers between co-authors for analysis. The succession of coating analysis was carefully planned to limit the possible interfering effects introduced by the analytical technique or by specimen preparation. The author himself investigated the coatings by scanning electron microscopy and energy dispersive spectroscopy. He also measured the roughness by confocal microscope and residual stress based on the curvature radius of coatings on the silicon substrate.

Data were curated and analyzed by the author, and he provided data visualization and illustrative figures. In cooperation with other co-authors, the author described the properties of Ta-B-C coating as a function of their composition and formulated the findings and hypothesis during fruitful meetings. The author wrote the original draft with assoc. prof. P. Souček and was responsible for the publication process including submission and revision.

4.3 Industrially deposited hard and damage resistant W-B-C coatings

DOI: not yet available

Published: after minor revision (November 2022)

Journal: Surface & Coating Technology

Impact factor in year of publication: 4.865

Authors: M. Kroker, P. Souček, L. Zábranský, Zs. Czigány, V. Sochora, K. Balázsi, M. Jílek and P. Vašina

Author's contribution:

Publication shares the research methodology and concept developed by the author in the publication 4.2. The author managed the cooperation on this publication with SHM, s.r.o., which provided the benchmark coatings for this publication.

The author conducted the W-B-C coatings depositions, including the sample preparation and curation. He analyzed coating morphology, cross-section, and residual imprints using scanning electron microscopy and confocal microscope and determined the composition of coatings by standard-based energy dispersive spectroscopy. The approach for the standard-based EDS was developed by the author to characterize the coating composition with high accuracy. It included finding proper parameters of spectra acquisition and preparing the suitable standard specimen as described in section 2.2.1. The author also performed an analysis of the residual stress.

Identification of crystalline phases was performed by the author from the selected area electron diffraction pattern using the CrystTBox suite [117] and Materials Project database of theoretical unit cells [102]. He interpreted the transmission electron investigation in cooperation with Dr. Zs. Czigány.

The damage resistance of the coatings was evaluated by measuring the damage parameter. The method was adapted for the coatings by the author's and assoc. prof. V. Buršíková's joint effort. They successfully utilized it to determine the differences between W-B-C coatings and nitride coatings and showed outstanding resistance of W-B-C coatings to the damage.

The author was responsible for data curation and analysis. He prepared all figures for visualization of data and findings. The original draft and following versions were written by the author based on the remarks of other co-authors. He also handled the submission and revision process.

4.4 Predicting the composition of W-B-C coatings sputtered from industrial cylindrical segmented target

DOI: 10.1016/j.surfcoat.2022.128411

Published: April 2022

Journal: Surface & Coatings Technology

Impact factor in year of publication: 4.865

Authors: M. Kroker, P. Souček, M. Šlapanská, and P. Vašina

Author's contribution:
The author proposed using a combination of SiMTra and SDTrimSP to predict the composition of the W-B-C coatings deposited from the cylindrical segmented target. Before the investigation, it was necessary to gain knowledge and experience with both codes, which enabled the author to develop Python-based frame software for the simulation of complex industrial systems with segmented targets composed of multiple materials.

The developed software was capable of generating inputs for the SiMTra simulation, running the simulations in batch, and extracting the data to obtain the composition and relative thickness of the coatings. The software also converted the outputs of the SDTrimSP to suit the SiMTra and derived the sputtering yields of the materials.

The author conducted the experimental work, including the coating deposition and analysis. He determined the composition by standard-based EDS and performed the calotest and confocal microscope analysis to derive the thickness of the coatings. Analysis and visualization of the magnetic field was performed by the author with Dr. M. Šlapanská utilizing the magnetic pole sensor foil.

The author created schematics of the simulation domain, illustrative figures, and data visualization, including the probability map of the racetrack and differential sputtering yields. The original draft and its finalized and revised version were compiled by the author with inputs from the all co-authors. He also handled whole submission process.

4.5 Co-authored publications

The co-authored publications are not directly connected to the topic of the doctoral research of the Me-B-C coatings. The focus on other research branches was driven by the author's curiosity and interest in the field of magnetron sputtering and associated low-temperature plasma physics. However, the contribution to the publications was also based on the knowledge gained from the author's doctoral research and the experience with deposition process simulation.

i) Single-shot spatial-resolved optical emission spectroscopy of argon and titanium species within the spoke

DOI: 10.1088/1361-6463/ac2cae

Published: October 2021

Journal: Journal of Physics D: Applied Physics

Impact factor in year of publication: 3.207

Authors: M. Šlapanská, M. Kroker, P. Klein, J. Hnilica and P. Vašina

Author's contribution:
In this publication, the author contributed mainly with technical experience from sputtering systems and related technical issues. The author was a consultant on the experiment design and technical approach to the plasma diagnostics. For the purpose of this publication, a homemade Langmuir probe and pre-amplified fast-photo diode apparatus were made to capture signals to detect moving ionization zones (the so-called spokes) on the titanium target during HiPIMS discharge.

The author was present during the experimental investigation, which included operating the sputtering system, HiPIMS generator, and Keysight DSOS204A high-end 4-channel oscilloscope. He participated in the data evaluation and interpretation and provided comments on the original draft.

ii) Spatially resolved study of spokes in reactive HiPIMS discharge

DOI: 10.1088/1361-6595/ac6a0c

Published: May 2022

Journal: Plasma Sources Science and Technology

Impact factor in year of publication: 3.584

Authors: M. Šlapanská, M. Kroker, P. Klein, J. Hnilica and P. Vašina

Author's contribution:

The author participated in the design of the experiment and conceptualization of this publication; he took part during the experimental investigation and aided the technical issues with the sputtering system and plasma diagnostics. He also participated in the data analysis and consulted their curation and processing by the automatic algorithm.

To help interpret the experimental observations, the author derived the sputtering yields of titanium targets utilizing the SDTrimSP. They included the self-sputtering yields and yields of multiply charged argon and nitrogen ions to attain possible sputtering events during reactive HiPIMS of titanium target with nitrogen as the reactive gas. The author contributed to several parts of the manuscript and commented on the original draft. He also participated in the minor revision of the manuscript.

iii) Modelling of dcMS and HiPIMS process with hydrocarbon gas admixture

DOI: 10.1088/1361-6595/ac7746

Published: July 2022

Journal: Plasma Sources Science and Technology

Impact factor in year of publication: 3.584

Authors: M. Fekete, M. Kroker, P. Souček, P. Klein and P. Vašina

Author's contribution:

The author contributed to this publication by calculating the energy-dependent sputtering yields of probable events that may occur during reactive HiPIMS of titanium target and acetylene as reactive gas.

With extensive experience with SDTrimSP code, the author developed a simulation of the target composition during the PVD-PECVD hybrid process. It simulated simultaneous sputtering of titanium targets by argon ions and adsorption of the thermalized carbon on the target. As a result, the depth-resolved composition of the target was derived, and the composition of the near-surface layer was determined, which corroborated the experimental results and validated the proposed model.

The author contributed to the original draft and the revised manuscript in the sections concerned with the SDTrimSP simulation and corresponding results.

Conclusions

The goal of the doctoral research was to study ternary metal-boron-carbon coatings prepared by an industrial deposition process. The research successfully derived experimental methods of coatings preparation and characterization, described the properties of tungsten- and tantalum-containing coatings, and studied the industrial deposition process. The key conclusions follow:

Combinatorial approach The cylindrical sputter source with a segmented target enabled depositing coatings with compositional gradient. The combinatorial approach was therefore achieved within the industrial batch-coater utilizing only single sputter source. The combinatorial approach allowed for studying the coating properties as a function of their composition while ensuring that process parameters were identical. It covered a wide composition range of the W-B-C and Ta-B-C coatings and reduced the count of necessary deposition processes. Therefore, it substantially sped up the research and lowered its cost.

Characterization methods Two analytical methodologies were introduced. They were developed to characterize the Me-B-C coatings properly, but they were also generally applicable to other coatings. The first methodology described standard-based energy dispersive spectroscopy and preparing suitable standards for the quantitative analysis. It enabled measuring coating composition with high accuracy and spotting minor differences in the composition between deposition regimes.

The second methodology described an approach for evaluating the coating's damage resistance. By utilizing the instrumental indentation technique with a cube-corner indenter tip, it was possible to determine the influence of the damage on the elastic response and quantify it for various types of coatings.

Ta-B-C coatings Several crystalline phases were observed in the Ta-B-C coatings. The ternary orthorhombic Ta_2BC crystalline phase was not proven. Only binary phases of tantalum were observed. The phase presence corresponded to the coating composition, and these were TaB, TaB_2, and TaC. The coatings' structure ranged from nanocrystalline to polycrystalline depending on the tantalum content. A fine multilayered structure formed in a 1-axis rotation regime limited the size of crystal grains.

The Ta-B-C coatings achieved very high hardness and elastic modulus, up to $\sim$35 GPa and $\sim$450 GPa, respectively. High compressive stress, however, significantly limited the maximal thickness of the coating and was causing cohesion failures. By observing the residual imprints after high-load indentation tests, the fracture resistance of the Ta-B-C coatings was concluded to be on par with the state-of-the-art nitride coatings. The Ta-B-C coatings in the studied composition range did not fulfill the expectations of enhanced fracture resistance.

W-B-C coatings Within the W-B-C coating system, the orthorhombic crystalline phase was not confirmed as well. High boron content favored the start of crystallization of tungsten boride and diboride, and the high carbon content resulted in the nanocrystalline coating with c-WC. But generally, the W-B-C coatings exhibited a low tendency to form any crystalline phase, and most prepared coatings were amorphous. Even so, their mechanical properties sort the amorphous W-B-C coatings among hard coatings.

The amorphous coating with W_2BC composition exhibited hardness of $\sim$25 GPa and elastic modulus of $\sim$400 GPa. The coating was stress-free and it was possible to deposit a coating with thickness larger than 40 µm without any adhesion or cohesion failure. The coating outperformed the nitride coatings in damage resistance, and the plastic deformation exhibited similarities to the ductile materials.

Inherent multilayering The research discovered and described inherently formed multi-layered structures of W-B-C and Ta-B-C coatings. The multilayering was confirmed to be a direct consequence of the substrate performing rotation movement during the deposition process.

The multilayering originated from distinct pathways of sputtered atoms of different elements during the transport from target to substrate. The mass of sputtered atoms had a decisive role in the type of transport. The light atoms were prone to high-angle scattering on working gas atoms, while the heavy atoms followed the more direct path. Therefore the coating composition depended on the substrate position and distance to the target.

The moving substrate thus passes through changing deposition fluxes that leads to modulation of the coating composition along the growth direction, which shows as the multilayered structure. While such multilayering is emphasized for coatings composed of elements with a considerable mass difference, it is expected to be present to some extent in every deposition process that utilizes any substrate motion.

Deposition process simulation Drawback of the segmented target setup was its complexity. The composition cannot be readily determined from the target setup, making it highly challenging to design the segmented target for the deposition of the desired coating.

It was overcome by developing the simulation approach, which could predict the coatings' composition from the target setup and process parameters. The simulation tool was based on the free-of-charge software SDTrimSP and SiMTra, which simulated the target sputtering and the particles transport. It was able to derive the composition and relative thickness of the coatings prepared in a complex setup of industrial batch-coater.

The calibration of the model on experimental results was still necessary, but the calibrated model provided a highly accurate prediction of the coating composition and relative thickness. The simulation tool was not limited solely to W-B-C and Ta-B-C coatings and was able to provide predictions for various segmented targets.

Appendices

Contents

MICHAEL KROKER

Contact

on request

kroker@physics.muni.cz

www.kroker.cz

in/michaelkroker/

Highlighted skills

- ✓ Experimental data processing & analysis
- ✓ Industry collaboration
- ✓ Results reporting
- ✓ SEM imaging
- ✓ Python programming

Technical skills

- ✓ High-vacuum systems
- ✓ SEM / TEM / EDS
- ✓ Raman spectroscopy
- ✓ XRD / SAED
- ✓ 3D profilometry
- ✓ Confocal microscopy

Hobbies

- Electronics
- Cycling
- Running
- Hiking

Profile

Ph.D. candidate at Masaryk University, Brno (Czech Republic)
Creative and problem-solving researcher
Highly experienced in results reporting
Ability to communicate with industrial partners and other associates

Education

2018 – present **Plasma Physics, Masaryk University**, Brno
Doctoral degree program
Thesis: *Magnetron sputtered hard ternary coatings with enhanced fracture toughness*

2016 – 2018 **Plasma Physics, Masaryk University**, Brno
Masters' degree program (Graduating with Honors)
Thesis: *Deposition and Characterization of Nanolaminates*

2013 – 2016 **Nanotechnology, Masaryk University**, Brno
Bachelor's degree program (Graduating with Honors)
Thesis: *Development of Industrial Technology for deposition of DLC Thin Films*

Work Experience

2019 – present **Researcher, Masaryk University**, Brno
Analysis and development of sputtered thin films.
Developing of industrial process to deposit nanolaminate ternary metal-boron-carbon coatings.

2015 – 2019 **Part-time cooperation, Masaryk University**, Brno
Member of a research group that focuses on magnetron sputtering. Specialization in thin film deposition, analysis of thin films and simulation of the sputtering process.

2013 – present **Network manager, IT support, ETOURS,** Uherské Hradiště
Management of computer network and technical support at a small company.

Skills

Experimental data processing, analysis, and results reporting

Confident in the use of graphing software like OriginLab as well as open-source QtiPlot, Plotly

Software development using Python and MATLAB

Simulation of magnetron sputtering process (SiMTra, SRIM/TRIM, SDTrimSP)

Highly skilled in SEM imaging and EDS chemical analysis

Experienced in IT support and company network deployment

MS Office (Word, Excel, PowerPoint, Access), LATEX, Web Design

Awards

Dean's Award for outstanding representation of the faculty

Werner von Siemens Award - Top thesis in the category Best diploma theses

Publications

Industrially deposited hard and damage resistant W-B-C coatings

KROKER, Michael, Pavel SOUČEK, Lukáš ZÁBRANSKÝ, Vilma BURŠÍKOVÁ, Zsolt CZIGÁNY, Vjačeslav SOCHORA, Katalin BALÁZSI, Mojmír JÍLEK & Petr VAŠINA
Surface & Coatings Technology (2023), after minor revision (November 2022)

Modelling of dcMS and HiPIMS process with hydrocarbon gas admixture

FEKETE, Matej, Michael KROKER, Pavel SOUČEK, Peter KLEIN & Petr VAŠINA
Plasma Sources Science and Technology **31** (2022), 065008

Spatially resolved study of spokes in reactive HiPIMS

ŠLAPANSKÁ, Marta, Michael KROKER, Peter KLEIN, Jaroslav HNILICA & Petr VAŠINA
Plasma Sources Science and Technology **31** (2022), 055010

Predicting the composition of W-B-C coatings sputtered from industrial cylindrical segmented target

KROKER, Michael, Pavel SOUČEK, Marta ŠLAPANSKÁ, Vjačeslav SOCHORA, Mojmír JÍLEK & Petr VAŠINA
Surface and Coatings Technology **438** (2022), 128411

Single-shot spatial-resolved optical emission spectroscopy of argon and titanium species within the spoke

ŠLAPANSKÁ, Marta, Michael KROKER, Jaroslav HNILICA, Peter KLEIN & Petr VAŠINA
Journal of Physics D: Applied Physics **55** (2022), 035205

Composition, structure and mechanical properties of industrially sputtered Ta–B–C coatings

KROKER, Michael, Pavel SOUČEK, Pavol MATEJ, Lukáš ZÁBRANSKÝ, Zsolt CZIGÁNY, Katalin BALÁZSI & Petr VAŠINA
Coatings **10(9)** (2020), 853

On the origin of multilayered structure of W-B-C coatings prepared by non-reactive magnetron sputtering from a single segmented target

KROKER, Michael, Zsolt CZIGÁNY, Zdeněk WEISS, Matej FEKETE, Pavel SOUČEK, Katalin BALÁZSI, Vjačeslav SOCHORA, Mojmír JÍLEK & Petr VAŠINA
Surface and Coatings Technology **377** (2019), 124864

Conference contributions

Industrial Deposition of W-B-C Coatings: Properties and Process Modelling
<ins>KROKER, Michael</ins>, Pavel SOUČEK, Lukáš ZÁBRANSKÝ, Vilma BURŠÍKOVÁ, Sochora VJAČESLAV, Mojmír JÍLEK & Petr VAŠINA.
48th International Conference on Metallurgical Coatings and Thin Films (2022)

Investigation of spokes in reactive Ar/N2 atmosphere using HiPIMS
KLEIN, Peter, Jaroslav HNILICA, Marta ŠLAPANSKÁ, Michael KROKER & Petr VAŠINA
25th Europhysics Conference on Atomic and Molecular Physics of Ionized Gases (2022)

Mapping the X-B-C Systems: Search for the Elusive X2BC Phase
SOUČEK, Pavel, Stanislava DEBNÁROVÁ, Mostafa ALISHAHI, Saeed MIRZAEI, <ins>Michael KROKER</ins>, Lukáš ZÁBRANSKÝ, Vilma BURŠÍKOVÁ, Zsolt CZIGÁNY, Katalin BALÁZSI, Marcus HANS, Damian HOLZAPFEL, Stanislav MRÁZ, Jochen Michael SCHNEIDER & Petr VAŠINA
48th International Conference on Metallurgical Coatings and Thin Films (2022)

Rotating spokes in reactive HiPIMS process measured by spatially resolved OES
ŠLAPANSKÁ, Marta, <ins>Michael KROKER</ins>, Jaroslav HNILICA, Peter KLEIN & Petr VAŠINA
48th International Conference on Metallurgical Coatings and Thin Films (2022)

Single-Shot Spatially Resolved Optical Emission Spectroscopy of Plasma Species within the Spoke
ŠLAPANSKÁ, Marta, Michael KROKER, Jaroslav HNILICA, Peter KLEIN & Petr VAŠINA
Plasma Processing and Technology International Conference 2021 (2021)

The Industrially Deposited W-B-C Coatings from Segmented Target
<ins>KROKER, Michael</ins>, Pavol MATEJ, Pavel SOUČEK, Lukáš ZÁBRANSKÝ, Vilma BURŠÍKOVÁ, Sochora VJAČESLAV, Mojmír JÍLEK & Petr VAŠINA
International Conference on Metallurgical Coatings and Thin Films (2021)

The single-shot spatial-resolved OES of the spoke in non-reactive HiPIMS
ŠLAPANSKÁ, Marta, <ins>Michael KROKER</ins>, Jaroslav HNILICA, Peter KLEIN & Petr VAŠINA
47th International Conference on Metallurgical Coatings and Thin Films (2021)

Hard and fracture resistant metal-boron-carbon based coatings deposited by industrial sputtering system
VAŠINA, Petr, <ins>Michael KROKER</ins>, Pavol MATEJ, Matej FEKETE, Lukáš ZÁBRANSKÝ, Pavel SOUČEK, Saeed MIRZAEI, Mostafa ALISHAHI, Vilma BURŠÍKOVÁ a Vjačeslav SOCHORA
Plathinium (2019)

On the origin of multilayered structure of W B C coatings prepared by non-reactive magnetron sputtering from a single segmented target
<ins>KROKER, Michael</ins>, Pavel SOUČEK, Matej FEKETE, Petr ZIKÁN, Adam OBRUSNÍK, Zsolt CZIGÁNY, Katalin BALÁZSI, Zdeněk WEISS & Petr VAŠINA.
46th International Conference on Metallurgical Coatings and Thin Films (2019)

Influence of chemical composition on structure and mechanical properties of W-B-C coating deposited in industrial sputtering system
VAŠINA, Petr, <ins>Michael KROKER</ins>, Matej FEKETE, Lukáš ZÁBRANSKÝ a Vilma BURŠÍKOVÁ.
83rd IUVSTA Workshop (2018)

Feasibility study of WBC synthesis from segmented magnetron target
<ins>KROKER, Michael</ins>, Pavel SOUČEK & Petr VAŠINA.
8th International Conference on Innovations in Thin Film Processing and Characterization (2017)

Properties of WBC coatings prepared by magnetron sputtering from industrial segmented target
<ins>KROKER, Michael</ins>, Pavel SOUČEK, Lukáš ZÁBRANSKÝ, Vilma BURŠÍKOVÁ & Petr VAŠINA
16th International Conference on Reactive Sputter Deposition (2017)

References

[1] GUDMUNDSSON, J. T. – LUNDIN, D. Introduction to magnetron sputtering. In *High Power Impulse Magnetron Sputtering*. Amsterdam, Netherlands: Elsevier, 2020. p. 1–48. doi: 10.1016/B978-0-12-812454-3.00006-1.

[2] SCHOLL, R. A. Power systems for reactive sputtering of insulating films. *Surface and Coatings Technology*. 1997, 93, 1, p. 7–13. doi: 10.1016/S0257-8972(97)00032-7.

[3] PEI, Y. T. et al. Microstructural control of TiC/a-C nanocomposite coatings with pulsed magnetron sputtering. *Acta Materialia*. 2008, 56, 4, p. 696–709. doi: 10.1016/j.actamat.2007.10.025.

[4] KOUZNETSOV, V. et al. A novel pulsed magnetron sputter technique utilizing very high target power densities. *Surface and Coatings Technology*. 1999, 122, 2-3, p. 290–293. doi: 10.1016/S0257-8972(99)00292-3.

[5] PAULITSCH, J. et al. Structure and properties of high power impulse magnetron sputtering and DC magnetron sputtering CrN and TiN fi lms deposited in an industrial scale unit. *Thin Solid Films*. 2010, 518, 19, p. 5558–5564. doi: 10.1016/j.tsf.2010.05.062.

[6] ANDERS, A. A structure zone diagram including plasma-based deposition and ion etching. *Thin Solid Films*. 2010, 518, 15, p. 4087–4090. doi: 10.1016/j.tsf.2009.10.145.

[7] MAHIEU, S. et al. Biaxial alignment in sputter deposited thin films. *Thin Solid Films*. 2006, 515, 4, p. 1229–1249. doi: 10.1016/j.tsf.2006.06.027.

[8] GREENE, J. E. Review Article: Tracing the recorded history of thin-film sputter deposition: From the 1800s to 2017. *Journal of Vacuum Science & Technology A: Vacuum, Surfaces, and Films*. 2017, 35, 5, p. 05C204. doi: 10.1116/1.4998940.

[9] POWELL, R. A. – ROSSNAGEL, S. M. *PVD for Microelectronics: Sputter Deposition Applied to Semiconductor Manufacturing (Thin Films)*. New York: Academic Press, 1998.

[10] LETERRIER, Y. et al. Mechanical integrity of transparent conductive oxide films for flexible polymer-based displays. *Thin Solid Films*. 2004, 460, 1-2, p. 156–166. doi: 10.1016/j.tsf.2004.01.052.

[11] MÜLLER, J. et al. TCO and light trapping in silicon thin film solar cells. *Solar Energy*. 2004, 77, 6, p. 917–930. doi: 10.1016/j.solener.2004.03.015.

[12] MARTIN, P. M. *Deposition technologies for films and coatings*. William Andrew, Elsevier, 2005. ISBN 9780815520313.

[13] ERLAT, A. G. et al. Characterisation of aluminium oxynitride gas barrier films. *Thin Solid Films*. 2001, 388, 1-2, p. 78–86. doi: 10.1016/S0040-6090(01)00836-7.

[14] KUZMINOVA, A. et al. Barrier Coatings on Polymeric Foils for Food Packaging. *Wds*. 2013, p. 128–133.

[15] BALDWIN, K. R. et al. Aluminium-magnesium alloys as corrosion resistant coatings for steel. *Corrosion Science*. 1996, 38, 1, p. 155–170. doi: 10.1016/0010-938X(96)00123-0.

[16] BUDINOVSKII, S. A. et al. Thermal-Barrier Coatings with an External Magnetron-Sputtered Ceramic Layer for High-Temperature Nickel Alloy Turbine Blades. *Russian Metallurgy (Metally)*. 2019, 2019, 6, p. 617–623. doi: 10.1134/S0036029519060090.

[17] MUSIL, J. Hard and superhard nanocomposite coatings. *Surface and Coatings Technology*. 2000, 125, 1-3, p. 322–330. doi: 10.1016/S0257-8972(99)00586-1.

[18] CERAC, INC. Optical Coating: Materials and Deposition Technology, 2022. Available at: `https://www.photonics.com/Articles/Optical_Coating_Materials_and_Deposition/a25493`.

[19] EDMUND OPTICS, LTD. An Introduction to Optical Coatings, 2022. Available at: `https://www.edmundoptics.eu/knowledge-center/application-notes/lasers/an-introduction-to-optical-coatings/`.

[20] RIGATO, V. et al. Properties of sputter-deposited MoS2/metal composite coatings deposited by closed field unbalanced magnetron sputter ion plating. *Surface and Coatings Technology*. 2000, 131, 1-3, p. 206–210. doi: 10.1016/S0257-8972(00)00797-0.

[21] OC OERLIKON BALZERS, AG. Coated components - Greater performance and reliability. Technical report, Oerlikon Balzers, Balzers, 2010. Available at: `https://www.oerlikon.com/ecoma/files/HQ040EN_Coated-Components.pdf`.

[22] ROSSNAGEL, S. M. Thin film deposition with physical vapor deposition and related technologies. *Journal of Vacuum Science & Technology A: Vacuum, Surfaces, and Films*. 2003, 21, 5, p. S74–S87. doi: 10.1116/1.1600450.

[23] ROSSNAGEL, S. M. Magnetron plasma diagnostics and processing implications Magnetron plasma diagnostics and processing implications. *Journal of Vacuum Science and Technology A*. 2008, 1821, 1988. doi: 10.1116/1.575262.

[24] KELLY, P. – ARNELL, R. Magnetron sputtering: a review of recent developments and applications. *Vacuum*. 2000, 56, 3, p. 159–172. doi: 10.1016/S0042-207X(99)00189-X.

[25] MUSIL, J. – VLCEK, J. – BAROCH, P. Magnetron Discharges for Thin Films Plasma Processing. *Materials Surface Processing by Directed Energy Techniques*. 2006, p. 67–110. doi: 10.1016/B978-008044496-3/50004-6.

[26] TIETEMA, R. – TECHNO, H. – BV, C. *Large-Scale Industrial Coating Applications and Systems*. 4. Elsevier, 2014. doi: 10.1016/B978-0-08-096532-1.00430-1.

[27] ZHANG, Z. – KHO, L. – WICKERSHAM, C. E. Effect of grain orientation on tantalum magnetron sputtering yield. *Journal of Vacuum Science & Technology A: Vacuum, Surfaces, and Films*. 2006, 24, 4, p. 1107–1111. doi: 10.1116/1.2212436.

[28] SCHNEIDER, J. M. et al. Role of hydrogen for the elastic properties of alumina thin films. *Applied Physics Letters*. 2002, 80, 7, p. 1144–1146. doi: 10.1063/1.1448389.

[29] LE FEBVRIER, A. et al. Effect of impurities on morphology, growth mode, and thermoelectric properties of (1 1 1) and (0 0 1) epitaxial-like ScN films. *Journal of Physics D: Applied Physics*. 2019, 52, 3. doi: 10.1088/1361-6463/aaeb1b.

[30] MÜLLER, C. M. et al. Nanoscale Cu/Ta multilayer deposition by co-sputtering on a rotating substrate. Empirical model and experiment. *Surface and Coatings Technology*. 2016, 302, p. 284–292. doi: 10.1016/j.surfcoat.2016.06.024.

[31] HANS, M. et al. Substrate rotation-induced chemical modulation in Ti-Al-O-N coatings synthesized by cathodic arc in an industrial deposition plant. *Surface and Coatings Technology*. 2016, 305, p. 249–253. doi: 10.1016/j.surfcoat.2016.08.046.

[32] BOBZIN, K. High-performance coatings for cutting tools. *CIRP Journal of Manufacturing Science and Technology*. aug 2017, 18, 2017, p. 1–9. doi: 10.1016/j.cirpj.2016.11.004.

[33] SUNDGREN, J. – HENTZELL, H. T. G. A review of the present state of art in hard coatings grown from the vapor phase. *Journal of Vacuum Science & Technology A: Vacuum, Surfaces, and Films*. 1986, 4, 5, p. 2259–2279. doi: 10.1116/1.574062.

[34] EMMERLICH, J. et al. A proposal for an unusually stiff and moderately ductile hard coating material: Mo2BC. *Journal of Physics D: Applied Physics*. 2009, 42, 18. doi: 10.1088/0022-3727/42/18/185406.

[35] BOLVARDI, H. et al. Systematic study on the electronic structure and mechanical properties of X2BC (X = Mo, Ti, V, Zr, Nb, Hf, Ta and W). *Journal of Physics Condensed Matter*. 2013, 25, 4. doi: 10.1088/0953-8984/25/4/045501.

[36] IVASHCHENKO, V. I. et al. Electronic origin of elastic properties of titanium carbonitride alloys. *Metallurgical and Materials Transactions A: Physical Metallurgy and Materials Science*. 2006, 37, 12, p. 3391–3396. doi: 10.1007/s11661-006-1031-9.

[37] RADNÓCZI, G. Hard coatings: state-of-the-art and applications. In *Microscopy of Tomorrow's Industrial Materials*, Berlin-Adlershof, Germany, 2005. International Centre of Advanced Materials Science and Electron Microscopy.

[38] MITTERER, C. PVD and CVD Hard Coatings. In *Comprehensive Hard Materials*, 2. Amsterdam, Netherlands: Elsevier Ltd, 2014. p. 449–467. doi: 10.1016/B978-0-08-096527-7.00035-0.

[39] JÄGER, N. et al. Impact of Si on the high-temperature oxidation of AlCr(Si)N coatings. *Journal of Materials Science & Technology*. feb 2022, 100, p. 91–100. doi: 10.1016/j.jmst.2021.04.065.

[40] WANG, F. et al. Systematic ab initio investigation of the elastic modulus in quaternary transition metal nitride alloys and their coherent multilayers. *Acta Materialia*. apr 2017, 127, p. 124–132. doi: 10.1016/j.actamat.2017.01.017.

[41] SOUČEK, P. et al. Superhard nanocomposite nc-TiC/a-C:H coatings: The effect of HiPIMS on coating microstructure and mechanical properties. *Surface and Coatings Technology*. 2017, 311, p. 257–267. doi: 10.1016/j.surfcoat.2017.01.021.

[42] PUGH, S. XCII. Relations between the elastic moduli and the plastic properties of polycrystalline pure metals. *The London, Edinburgh, and Dublin Philosophical Magazine and Journal of Science*. aug 1954, 45, 367, p. 823–843. doi: 10.1080/14786440808520496.

[43] SENKOV, O. N. – MIRACLE, D. B. Generalization of intrinsic ductile-to-brittle criteria by Pugh and Pettifor for materials with a cubic crystal structure. *Scientific Reports*. 2021, 11, 1, p. 10–13. doi: 10.1038/s41598-021-83953-z.

[44] RZEPIEJEWSKA-MALYSKA, K. et al. In situ scanning electron microscopy indentation studies on multilayer nitride films: Methodology and deformation mechanisms. *Journal of Materials Research*. mar 2009, 24, 3, p. 1208–1221. doi: 10.1557/jmr.2009.0139.

[45] QUINN, G. D. *Fractography of Glasses and Ceramics V*. 199 / *Ceramic Transactions Series*. Wiley, jul 2007. doi: 10.1002/9781118144152.

[46] VOEVODIN, A. A. et al. (Ed.). *Nanostructured Thin Films and Nanodispersion Strengthened Coatings*. 155 / *NATO Science Series II: Mathematics, Physics and Chemistry*. Springer Netherlands, 2004. doi: 10.1007/1-4020-2222-0.

[47] BROOKES, K. J. – LÜMKEMANN, A. PLATIT-pioneers in physical vapour deposition. *Metal Powder Report*. 2013, 68, 2, p. 24–27. doi: 10.1016/S0026-0657(13)70060-2.

[48] JEITSCHKO, W. – NOWOTNY, H. – BENESOVSKY, F. Die Kristallstruktur von Mo2BC. *Monatshefte für Chemie*. 1963, 94, 3, p. 565–568. doi: 10.1007/BF00903497.

[49] BOVIN, J. O. – O'KEEFFE, M. – STENBERG, L. Planar defects in Mo2BC. An electron microscope study. *Journal of Solid State Chemistry*. 1977, 22, 2, p. 221–231. doi: 10.1016/0022-4596(77)90041-X.

[50] LEJAY, P. et al. The borocarbides Mo(2-x)W(x)BC ($0 \leq x \leq 1.1$), a new family of refractory superconducting materials. *Synthetic Metals*. dec 1981, 4, 2, p. 139–145. doi: 10.1016/0379-6779(81)90029-1.

[51] EKLUND, P. et al. The M(n+1)AX(n) phases: Materials science and thin-film processing. *Thin Solid Films*. 2010, 518, 8, p. 1851–1878. doi: 10.1016/j.tsf.2009.07.184.

[52] BARSOUM, M. W. – RADOVIC, M. Elastic and mechanical properties of the MAX phases. *Annual Review of Materials Research*. 2011, 41, p. 195–227. doi: 10.1146/annurev-matsci-062910-100448.

[53] CASTAING, R. *Electron Probe Microanalysis*. 13 / *Advances in Electronics and Electron Physics*. Academic Press, 1960. doi: 10.1016/S0065-2539(08)60212-7.

[54] OXFORD INSTRUMENTS. AZtec Suite, 2022. Available at: `https://nano.oxinst.com/products/sem-and-fib`.

[55] BRUKER SCIENTIFIC INSTRUMENTS. ESPRIT, 2022. Available at: `https://www.bruker.com/en/products-and-solutions/elemental-analyzers/eds-wds-ebsd-SEM-Micro-XRF/software-esprit-family.html`.

[56] RITCHIE, N. W. M. NIST DTSA-II, 2018. Available at: `https://www.nist.gov/services-resources/software/nist-dtsa-ii`.

[57] HUBBELL, J. H. – SELTZER, S. M. Tables of X-Ray Mass Attenuation Coefficients and Mass Energy-Absorption Coefficients from 1 keV to 20 MeV for Elements Z = 1 to 92 and 48 Additional Substances of Dosimetric Interest*. *NIST Standard Reference Database 126*. 2004. doi: 10.18434/T4D01F.

[58] WEHNER, G. K. Sputtering of multicomponent materials. *Journal of Vacuum Science & Technology A: Vacuum, Surfaces, and Films*. apr 1983, 1, 2, p. 487–490. doi: 10.1116/1.571911.

[59] NEWBURY, D. E. – RITCHIE, N. W. Performing elemental microanalysis with high accuracy and high precision by scanning electron microscopy/silicon drift detector energy-dispersive X-ray spectrometry (SEM/SDD-EDS). *Journal of Materials Science*. 2014, 50, 2, p. 493–518. doi: 10.1007/s10853-014-8685-2.

[60] IRWIN, G. R. Analysis of Stresses and Strains Near the End of a Crack Traversing a Plate. *Journal of Applied Mechanics*. sep 1957, 24, 3, p. 361–364. doi: 10.1115/1.4011547.

[61] OTERKUS, E. et al. 4 - Fracture modes, damage tolerance and failure mitigation in marine composites. In GRAHAM-JONES, J. – SUMMERSCALES, J. (Ed.) *Marine Applications of Advanced Fibre-Reinforced Composites*. Sawston, UK: Woodhead Publishing, 2016. p. 79–102. doi: 10.1016/B978-1-78242-250-1.00004-1.

[62] PETTIFOR, D. G. Theoretical predictions of structure and related properties of intermetallics. *Materials Science and Technology*. apr 1992, 8, 4, p. 345–349. doi: 10.1179/mst.1992.8.4.345.

[63] LEYLAND, A. – MATTHEWS, A. On the significance of the H/E ratio in wear control: a nanocomposite coating approach to optimised tribological behaviour. *Wear*. nov 2000, 246, 1-2, p. 1–11. doi: 10.1016/S0043-1648(00)00488-9.

[64] MUSIL, J. et al. Relationships between hardness, Young's modulus and elastic recovery in hard nanocomposite coatings. *Surface and Coatings Technology*. may 2002, 154, 2-3, p. 304–313. doi: 10.1016/S0257-8972(01)01714-5.

[65] MUSIL, J. Flexible hard nanocomposite coatings. *RSC Advances*. 2015, 5, 74, p. 60482–60495. doi: 10.1039/c5ra09586g.

[66] CHEN, X. – DU, Y. – CHUNG, Y. W. Commentary on using H/E and H3/E2 as proxies for fracture toughness of hard coatings. *Thin Solid Films*. 2019, 688, April, p. 137265. doi: 10.1016/j.tsf.2019.04.040.

[67] LAWN, B. R. – EVANS, A. G. – MARSHALL, D. B. Elastic/Plastic Indentation Damage in Ceramics: The Median/Radial Crack System. *Journal of the American Ceramic Society*. sep 1980, 63, 9-10, p. 574–581. doi: 10.1111/j.1151-2916.1980.tb10768.x.

[68] ANSTIS, G. et al. A Critical Evaluation of Indentation Techniques for Measuring Fracture Toughness: I, Direct Crack Measurements. *Journal of the American Ceramic Society*. sep 1981, 64, 9, p. 533–538. doi: 10.1111/j.1151-2916.1981.tb10320.x.

[69] LAUGIER, M. T. New formula for indentation toughness in ceramics. *Journal of Materials Science Letters*. 1987, 6, 3, p. 355–356. doi: 10.1007/BF01729352.

[70] PHARR, G. Measurement of mechanical properties by ultra-low load indentation. *Materials Science and Engineering: A*. sep 1998, 253, 1-2, p. 151–159. doi: 10.1016/S0921-5093(98)00724-2.

[71] GREEN, D. J. – MALONEY, B. R. Influence of Surface Stress on indentation Cracking. *Journal of the American Ceramic Society*. mar 1986, 69, 3, p. 223–225. doi: 10.1111/j.1151-2916.1986.tb07412.x.

[72] JAYA, B. N. – KIRCHLECHNER, C. – DEHM, G. Can microscale fracture tests provide reliable fracture toughness values? A case study in silicon. *Journal of Materials Research*. 2015, 30, 5, p. 686–698. doi: 10.1557/jmr.2015.2.

[73] MAYER, C. et al. Anisotropy, size, and aspect ratio effects on micropillar compression of Al SiC nanolaminate composites. *Acta Materialia*. aug 2016, 114, p. 25–32. doi: 10.1016/j.actamat.2016.05.018.

[74] BEST, J. P. et al. High temperature fracture toughness of ceramic coatings evaluated using micro-pillar splitting. *Scripta Materialia*. mar 2019, 162, p. 190–194. doi: 10.1016/j.scriptamat.2018.11.013.

[75] ZÁBRANSKÝ, L. et al. The Effect of a Taper Angle on Micro-Compression Testing of Mo-B-C Coatings. *Materials*. jul 2020, 13, 14, p. 3054. doi: 10.3390/ma13143054.

[76] CUADRADO, N. et al. Geometry of nanoindentation cube-corner cracks observed by FIB tomography: Implication for fracture resistance estimation. *Journal of the European Ceramic Society*. 2015, 35, 10, p. 2949–2955. doi: 10.1016/j.jeurceramsoc.2015.03.031.

[77] AST, J. et al. A review of experimental approaches to fracture toughness evaluation at the micro-scale. *Materials and Design*. 2019, 173, p. 107762. doi: 10.1016/j.matdes.2019.107762.

[78] LIU, J. et al. Effect of Ion Irradiation Introduced by Focused Ion-Beam Milling on the Mechanical Behaviour of Sub-Micron-Sized Samples. *Scientific Reports*. 2020, 10, 1, p. 1–8. doi: 10.1038/s41598-020-66564-y.

[79] ZENG, K. – ROWCLIFFE, D. Analysis of penetration curves produced by sharp indentations on ceramic materials. *Philosophical Magazine A*. nov 1996, 74, 5, p. 1107–1116. doi: 10.1080/01418619608239711.

[80] AST, J. – GÖKEN, M. – DURST, K. Size-dependent fracture toughness of tungsten. *Acta Materialia*. 2017, 138, p. 198–211. ISSN 13596454. doi: 10.1016/j.actamat.2017.07.030.

[81] BRUNS, S. et al. Fracture toughness determination of fused silica by cube corner indentation cracking and pillar splitting. *Materials & Design*. 2020, 186, p. 108311. ISSN 02641275. doi: 10.1016/j.matdes.2019.108311.

[82] BOR, B. et al. Nanoindentation-based study of the mechanical behavior of bulk supercrystalline ceramic-organic nanocomposites. *Journal of the European Ceramic Society*. aug 2019, 39, 10, p. 3247–3256. doi: 10.1016/j.jeurceramsoc.2019.03.053.

[83] CLARIVATE. Web of Science, 2022. Available at: `https://www.webofscience.com`.

[84] BOLVARDI, H. et al. Low temperature synthesis of Mo2BC thin films. *Thin Solid Films*. 2013, 542, p. 5–7. doi: 10.1016/j.tsf.2013.07.021.

[85] DJAZIRI, S. et al. Are Mo2BC nanocrystalline coatings damage resistant? Insights from comparative tension experiments. *Surface and Coatings Technology*. 2016, 289, p. 213–218. doi: 10.1016/j.surfcoat.2016.02.010.

[86] SOLER, R. et al. Fracture toughness of Mo2BC thin films: Intrinsic toughness versus system toughening. *Materials and Design*. 2018, 154, p. 20–27. doi: 10.1016/j.matdes.2018.05.015.

[87] ZÁBRANSKÝ, L. et al. On the study of the mechanical properties of Mo-B-C coatings. *The European Physical Journal Applied Physics*. aug 2016, 75, 2, p. 24716. doi: 10.1051/epjap/2016150591.

[88] SOUCEK, P. et al. Fracture Resistance Enhancement in Hard Mo-B-C Coatings Tailored by Composition and Microstructure. *Journal of Nanomaterials*. 2018, 2018, p. 1–7. doi: 10.1155/2018/5184584.

[89] GLEICH, S. et al. Modifying the nanostructure and the mechanical properties of Mo2BC hard coatings: Influence of substrate temperature during magnetron sputtering. *Materials and Design*. 2018, 142, p. 203–211. doi: 10.1016/j.matdes.2018.01.029.

[90] FRIEDEMANN, M. – KLOSTERMANN, H. Composition and mechanical properties of B-C-W and B-C-Ti thin films prepared by pulse magnetron sputtering. *Surface and Coatings Technology*. 2016, 308, p. 115–120. doi: 10.1016/j.surfcoat.2016.07.107.

[91] ALISHAHI, M. et al. Evolution of structure and mechanical properties of hard yet fracture resistant W-B-C coatings with varying C/W ratio. *Surface and Coatings Technology*. 2018, 340, December 2017, p. 103–111. doi: 10.1016/j.surfcoat.2018.02.054.

[92] MIRZAEI, S. et al. Effect of bonding structure on hardness and fracture resistance of W-B-C coatings with varying B/W ratio. *Surface and Coatings Technology*. 2019, 358, June 2018, p. 843–849. doi: 10.1016/j.surfcoat.2018.12.007.

[93] MIRZAEI, S. et al. The effect of chemical composition on the structure, chemistry and mechanical properties of magnetron sputtered W-B-C coatings: Modeling and experiments. *Surface and Coatings Technology*. 2020, 383, September 2019, p. 125274. doi: 10.1016/j.surfcoat.2019.125274.

[94] DEBNÁROVÁ, S. et al. Study of W-B-C thin films prepared by magnetron sputtering using a combinatorial approach. *International Journal of Refractory Metals and Hard Materials*. 2019, 85, May. doi: 10.1016/j.ijrmhm.2019.105066.

[95] WICHER, B. et al. Design of pulsed neon injection in the synthesis of W-B-C films using magnetron sputtering from a surface-sintered single powder cathode. *Thin Solid Films*. 2020, 716, November. doi: 10.1016/j.tsf.2020.138426.

[96] DEBNÁROVÁ, S. et al. The tribological properties of short range ordered W-B-C protective coatings prepared by pulsed magnetron sputtering. *Surface and Coatings Technology*. 2019, 357, October 2018, p. 364–371. doi: 10.1016/j.surfcoat.2018.10.026.

[97] BURŠÍK, J. et al. Characterization of Ta-B-C nanostructured hard coatings. *IOP Conference Series: Materials Science and Engineering*. feb 2017, 175, 1, p. 012020. doi: 10.1088/1757-899X/175/1/012020.

[98] POLAČEK, M. et al. Synthesis and characterization of Ta–B–C coatings prepared by DCMS and HiPIMS co-sputtering. *Vacuum*. 2022, 199, February. doi: 10.1016/j.vacuum.2022.110937.

[99] DEBNÁROVÁ, S. et al. Phase formation, thermal stability and mechanical properties of Nb-B-C coatings prepared by combinatorial magnetron sputtering. *Surface and Coatings Technology*. 2022, 433, November 2021. doi: 10.1016/j.surfcoat.2022.128137.

[100] PANJAN, P. et al. Review of Growth Defects in Thin Films Prepared by PVD Techniques. *Coatings*. 2020, 10, 5, p. 447. doi: 10.3390/coatings10050447.

[101] CSELLE, T. Compendium 62nd Edition. Technical report, PLATIT AG., 2021. Available at: `https://www.platit.com/media/filer/2021/compendium_en62.pdf`. Page 12.

[102] JAIN, A. et al. Commentary: The materials project: A materials genome approach to accelerating materials innovation. *APL Materials*. 2013, 1, 1. doi: 10.1063/1.4812323.

[103] ASHIDA, S. – LEE, C. – LIEBERMAN, M. A. Spatially averaged (global) model of time modulated high density argon plasmas. *Journal of Vacuum Science & Technology A: Vacuum, Surfaces, and Films*. sep 1995, 13, 5, p. 2498–2507. doi: 10.1116/1.579494.

[104] MUSIC, D. – GEYER, R. W. – SCHNEIDER, J. M. Recent progress and new directions in density functional theory based design of hard coatings. *Surface and Coatings Technology*. 2016, 286, p. 178–190. doi: 10.1016/j.surfcoat.2015.12.021.

[105] BANKO, L. et al. Predicting structure zone diagrams for thin film synthesis by generative machine learning. *Communications Materials*. dec 2020, 1, 1, p. 15. doi: 10.1038/s43246-020-0017-2.

[106] ZIEGLER, J. F. – ZIEGLER, M. D. – BIERSACK, J. P. SRIM - The stopping and range of ions in matter (2010). *Nuclear Instruments and Methods in Physics Research, Section B: Beam Interactions with Materials and Atoms*. 2010, 268, 11-12, p. 1818–1823. doi: 10.1016/j.nimb.2010.02.091.

[107] MÖLLER, W. – ECKSTEIN, W. Tridyn — A TRIM simulation code including dynamic composition changes. *Nuclear Instruments and Methods in Physics Research Section B: Beam Interactions with Materials and Atoms*. mar 1984, 2, 1-3, p. 814–818. doi: 10.1016/0168-583X(84)90321-5.

[108] MUTZKE, A. et al. SDTrimSP Version 6.00. *(IPP 2019-02). Garching: Max-Planck-Institut für Plasmaphysi*. 2019.

[109] HOFSÄSS, H. – ZHANG, K. – MUTZKE, A. Simulation of ion beam sputtering with SDTrimSP, TRIDYN and SRIM. *Applied Surface Science*. 2014, 310, p. 134–141. doi: 10.1016/j.apsusc.2014.03.152.

[110] THOMPSON, M. W. II. The energy spectrum of ejected atoms during the high energy sputtering of gold. *Philosophical Magazine*. 1968, 18, 152, p. 377–414. doi: 10.1080/14786436808227358.

[111] BIZYUKOV, I. – MUTZKE, A. – SCHNEIDER, R. Effect of increasing surface roughness on sputtering and reflection. *Problems of Atomic Science and Technology*. 2012, 82, 6, p. 111–113. ISSN 16829344.

[112] FAN, Q. H. – ZHOU, L. Q. – GRACIO, J. J. A cross-corner effect in a rectangular sputtering magnetron. *Journal of Physics D: Applied Physics*. feb 2003, 36, 3, p. 244–251. doi: 10.1088/0022-3727/36/3/305.

[113] MUSSCHOOT, J. et al. Influence of the geometrical configuration on the plasma ionization distribution and erosion profile of a rotating cylindrical magnetron: a Monte Carlo simulation. *Journal of Physics D: Applied Physics*. sep 2006, 39, 18, p. 3989–3993. doi: 10.1088/0022-3727/39/18/010.

[114] VAN AEKEN, K. – MAHIEU, S. – DEPLA, D. The metal flux from a rotating cylindrical magnetron: A Monte Carlo simulation. *Journal of Physics D: Applied Physics*. 2008, 41, 20. doi: 10.1088/0022-3727/41/20/205307.

[115] ANDERS, A. Discharge physics of high power impulse magnetron sputtering. *Surface and Coatings Technology*. jul 2011, 205, SUPPL. 2, p. S1–S9. doi: 10.1016/j.surfcoat.2011.03.081.

[116] HIPPLER, R. et al. Pressure dependence of singly and doubly charged ion formation in a HiPIMS discharge. *Journal of Applied Physics*. jan 2019, 125, 1, p. 013301. doi: 10.1063/1.5055356.

[117] KLINGER, M. More features, more tools, more CrysTBox. *Journal of Applied Crystallography*. aug 2017, 50, 4, p. 1226–1234. doi: 10.1107/S1600576717006793.